Bone 121 (2019) 42–59

Contents lists available at ScienceDirect

Bone

journal homepage: www.elsevier.com/locate/bone

Full Length Article

Correlations between gene expression and mineralization in the avian leg tendon

Ling Chen, Robin DiFeo Childs, William J. Landis*

Department of Polymer Science, University of Akron, Akron, OH, USA

ARTICLE INFO

Keywords:
Gene expression
Mineralization
qPCR
Avian leg tendon

ABSTRACT

Certain avian tendons have been studied previously as a model system for normal mineralization of vertebrates in general. In this regard, the gastrocnemius tendon in the legs of turkeys mineralizes in a well defined temporal and spatial manner such that changes in the initial and subsequent events of mineral formation can be associated with time and specific locations in the tissue. In the present investigation, these parameters and mineral deposition have been correlated with the expression of several genes and the synthesis and secretion of their related extracellular matrix proteins by the composite tenocytes of the tendon. Quantitative polymerase chain reaction analysis demonstrates that mRNA expression of the non-collagenous genes of bone sialoprotein, osteopontin, and osteocalcin corresponds well with the temporal and spatial onset and progression of mineralization. Immunolocalization separately confirms the synthesis and secretion of these matrix molecules. The expression of other non-collagenous genes such as decorin does not show strong correlation with turkey leg tendon mineralization, and expression of vimentin, a cytoskeletal component which may be regulated by biomechanical factors in the tendon, may lead to inhibition of osteocalcin expression during the development and mineralization of the tissue. The overall results of this work provide insight into direct temporal and spatial relations between the genes and proteins of interest as well as the formation and deposition of mineral in the avian tendon model.

1. Introduction

The vertebrate skeletal tissues such as bones and teeth serve multiple physiological purposes, including, for example, their ability to provide mechanical strength and structural support, serving as a reservoir for ions, trace elements and small molecules, and maintaining homeostasis in the body [1]. The basis, in part, for these numerous and diverse roles is the chemistry and biomechanics of the mineral and the nature and interaction of its composite inorganic and organic phases. The principal, mature inorganic phase is an apatite while the organic phase contains collagen, non-collagenous proteins (NCPs), and other molecules such as proteoglycans. In general, it is believed that interactions between charged organic components of the tissues and oppositely charged ions such as Ca^{2+} and PO_4^{3-} in their supersaturated extracellular tissue fluids regulate nucleation, growth and development of the apatite crystals. To understand these interactions and possible roles of organic tissue components in mineralization more completely, the structure of the organic constituents has been studied in various systems in vitro [2–9] and in vivo [10–20]. However, the exact functions of many individual matrix components are still uncertain because of several factors such as investigations of different model systems or the use of varying methodologies or experimental conditions, all generating results that are difficult to compare. Different studies in vitro, in addition, propose inconsistent roles for the same NCP during the mineralization process [3,21] and, in occasional cases, skeletal development in vivo does not necessarily demonstrate expected phenotypic changes in knockout mice with a specific deleted gene(s) affecting a corresponding NCP(s) [22–26].

Mineral formation in vertebrates is highly regulated spatially and temporally by the organic matrix deposited in the tissues, a result suggesting correlation between gene expression, secretion of proteins and other molecules comprising the matrix, the timing and location of mineral deposition, and tissue structure and composition [27–29]. These several considerations are each complex, and only a few studies [28,30,31] have undertaken analysis of some of them together. Most investigations rather have examined one or two aspects separately, such as certain spatial or temporal events [32–35]. For example, temporal deposition profiles of major matrix components involved in mineralization are obtained from

* Corresponding author at: Department of Polymer Science, Goodyear Polymer Center, Room 1201C, University of Akron, 170 University Avenue, Akron, OH 44325-3909, USA.
E-mail address: wlandis@uakron.edu (W.J. Landis).

https://doi.org/10.1016/j.bone.2018.11.005
Received 12 June 2018; Received in revised form 2 November 2018; Accepted 7 November 2018
Available online 09 November 2018
8756-3282/ © 2018 Elsevier Inc. All rights reserved.

either work in vitro with osteogenic cell cultures [36,37] or studies in vivo investigating embryonic or neonatal development of mineralizing tissues [30,38,39]. Gene expression analysis by in situ hybridization and corresponding protein immunolocalization help identify and elucidate the spatial distribution of these matrix components in mineralized tissues [32–35]. However, the level of protein deposition is not always consistent with gene expression since protein abundance is regulated by post-transcriptional, translational, and degradation processes and other factors [40,41]. Thus, for detailing more precisely the numerous events leading to mineralization of a tissue, there is a definitive necessity to correlate gene expression, secretion of matrix components, and mineral formation and progression in both time and location. Such a correspondence should be done in a single system that avails itself to analyses of these multiple components and factors.

Avian tendons, especially turkey leg tendons (TLT), represent a model system for studying vertebrate mineralization in the context just noted [20,27,42–51]. Related temporal and spatial events are accessible in this particular tissue and they have been described in several studies that document its sequential, gradual mineralization in time and location [27,42,47,49,50]. Briefly, the Achilles, or gastrocnemius, tendon in the domestic turkey bifurcates at a point proximal to a principal joint in its upper legs. With aging, mineral deposition begins in the vicinity of the tendon branching and it proceeds spatially and temporally toward two proximal hip muscles into which the tendon segments insert in the animal [27]. Thus, at a given time during normal turkey and tendon development and maturation, there is a very well defined and regulated pattern of mineralization in the tissue such that older and younger events of mineral formation occur distally and proximally, respectively, relative to the gastrocnemius bifurcation point. By examining the TLT in a distal-to-proximal direction from the branching location, the various stages of mineralization can be carefully and precisely followed and analyzed spatially and temporally, as has been done in many earlier reports [27,42,47,49–51].

Previous investigation has demonstrated that NCPs are present in TLT and they may mediate the mineralization of its collagen-based matrix [52]. This paper attempts to correlate gene expression with certain morphological features during structural development, especially the mineralizing regions, of the TLT [50,52]. The work also addresses the question of the origin of the NCPs of interest and whether they are secreted by local tendon cells or delivered through the vasculature from external sources [53]. In the present study, the TLT is further examined to obtain additional results relating gene expression and secretion of type I collagen (TI COL), certain NCPs and other molecules, in this case bone sialoprotein (BSP), osteocalcin (OC), osteopontin (OPN), decorin (DCN), and vimentin (VIM), with respect to their time of appearance with animal age and tendon maturation and location as mineralization events proceed in this tissue. To the knowledge of the authors, no other study has reported in the same model system, in this case the normally mineralizing TLT, a correlation between the expression of certain genes and their counterpart secreted extracellular matrix proteins and other molecules and the spatial and temporal pattern of mineral formation in this tissue.

2. Materials and methods

2.1. Initial processing

Seven 12-week-old and three 15-week-old male domestic turkeys (*Meleagris gallopavo*) were obtained from a local farm (Hawk Farms, East Rochester, OH) and freshly sacrificed. The gastrocnemius tendons were dissected from their legs and the muscles attached to the tendons were carefully removed [27]. The tendon tissues from the left legs of all turkeys were immediately cut into small specimen segments having dimensions ~5 or 10 mm in width and length. The segments of 10 mm widths were taken on dissection of tendon regions proximal to the normal point of bifurcation of this tendon and 5 mm widths for regions distal to the bifurcation (Fig. 1). Individual segments were evenly spaced along the lengths of tendon proximal and distal aspects and identified as to their right (R) aspect or branch inserting into the *M. caput mediale* in the shank of the animal or their left (L) aspect or branch inserting into the *M. caput caudale* in the shank of the animal (Fig. 1). Segments spaced 10 mm apart in tendon regions proximal to the bifurcation point were numbered 1–5 in a proximal-to-distal direction along the R aspect and 6–10 along the L aspect of the tissue. Distal to the bifurcation, tendon regions were spaced 5 mm apart, divided in half

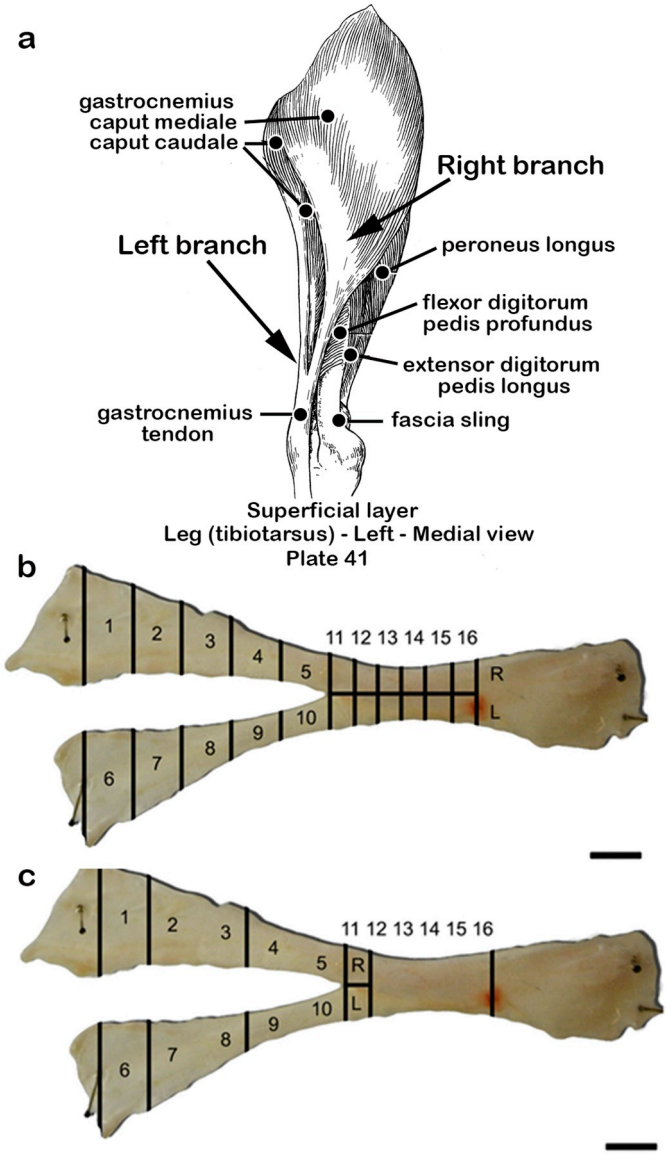

Fig. 1. Illustration and schematic of aspects of the normal gastrocnemius tendon from a 15-week-old domestic turkey. (a) An anatomical sketch of the gastrocnemius tendon and muscles into which the gastrocnemius inserts, adapted from Harvey et al. [57]. The distal portion of the tissue bifurcates as it passes through a sheath behind the joint of the turkey leg and the divided tendon branches insert proximally into either the *M. caput mediale* or *M. caput caudale*. (b) Specific regions of the tendon were dissected into numbered segments ~5 to 10 mm in width and length depending on location and subjected to gene expression study using RT-qPCR analysis. The right branch (R) of the tendon inserting into the *M. caput mediale* consisted of segments 1–5 and 11R–16R while the left branch (L) inserting into the *M. caput caudale* consisted of segments 6–10 and 11L–16L. Segments 1 and 6 were most proximal and segment 16 was most distal in the tissue. (c) Segments of the tendon in (b) grouped for the sake of simplicity for statistical analysis and comparison. Scale bar: 10 mm.

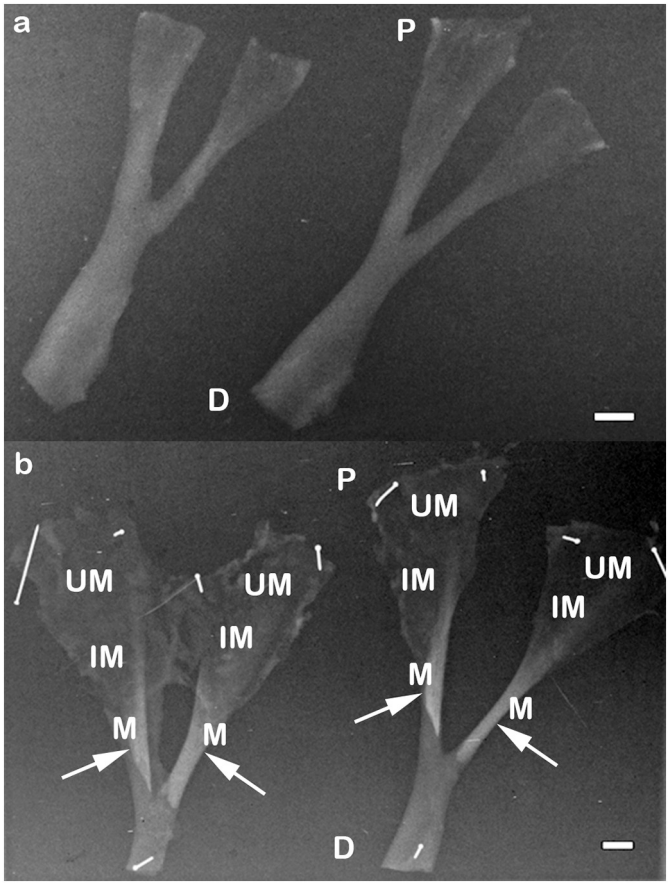

Fig. 2. X-ray radiographs of dissected gastrocnemius tendons from (a) 12-week-old turkeys and (b) 15-week-old turkeys. Radiopaque regions (solid arrows and M) shown in 15-week-old turkey tendons are mineralized tendon zones, each proximal to the point of tendon bifurcation. Two other principal proximal regions in these specimens are those that are presently unmineralized (UM) and those beginning to mineralize (IM, incipient mineralization detected by TEM [27] between unmineralized zones and the more distal, radiopaque mineralized zones). X-ray radiography does not reveal mineralization just distal to the bifurcation point in 15-week-old tendons or throughout 12-week-old tendons. Small radiopaque pins in (b) hold the tendons at various points to underlying paraffin blocks. P, proximal; D, distal. Scale bar: 10 mm.

longitudinally, and numbered 11–16 in a proximal-to-distal direction in each of the R and L aspects (Fig. 1). The tendon segments were immersed in Ambion RNA*later*™ solution (Ambion, Thermo Fisher Scientific, Inc., Waltham, MA), kept at 4 °C in a refrigerator for 24 h, and then stored at −80 °C for later gene expression analysis.

Four unsegmented gastrocnemius tendons from the right legs of four different turkeys, two from each age, were placed in flat, plastic containers and pinned to paraffin hardened in them (Fig. 2). The remaining six tendons from the right legs of the turkeys were utilized for additional studies reported elsewhere [52]. The four tendons pinned to paraffin were immersed in a fixative solution containing 4% paraformaldehyde and 1% or 2.5% glutaraldehyde in 0.1 M cacodylate buffer (pH 7.4, Electron Microscopy Sciences, Hatfield, PA). Containers were sealed with covers and the tendon specimens were transported to the laboratory on ice for further processing. These samples were investigated by X-ray radiography, immunocytochemistry and transmission electron microscopy.

2.2. X-ray radiography

The fixed tendons were removed from their paraffin containers and imaged by X-ray radiography to identify any mineralizing regions in the tissues. Radiography utilized an X-ray collimator (Model CM-1100, Huestis Medical, Bristol, RI) and radiograms were recorded on Fujifilm medical X-ray films (FUJIFILM Medical Systems U.S.A., Inc., Stamford, CT). Radiography showed that tendons from 12-week-old birds had not yet mineralized (Fig. 2a). Three principal regions from 15-week-old turkeys were defined by X-ray radiography as unmineralized, beginning to mineralize and already mineralized (Fig. 2b), and each such region was dissected and processed for immunocytochemistry of selected constituent NCPs, particularly BSP and OC.

2.3. Immunocytochemistry and transmission electron microscopy (TEM)

Immunocytochemistry utilized post-embedding immunolocalization viewed by TEM. Rabbit polyclonal antibodies against chicken OC and BSP were received as kind gifts from Dr. Louis Gerstenfeld (Boston University, Boston, MA) and Dr. Marc McKee (McGill University, Montreal, Canada), respectively. For the preparation of the primary antibody solution, the as-received OC antibodies were diluted (1:20) in 0.1 × PBS containing 2 mM Ca^{2+}. BSP antibodies were diluted (1:10) in 1 × phosphate buffered saline (PBS; stock solution without calcium and magnesium; VWR Int., Radnor, PA). Controls for antibody staining used 1 × PBS replacing antibody solutions. Immunolocalization of BSP and OC followed a previous protocol [45]. Briefly, the fixed tissues were dehydrated, infiltrated, and embedded in LR-white resin (hard grade; Electron Microscopy Sciences). Thin sections were cut using an ultramicrotome (Reichert Ultracut S, Leica Microsystems, Inc., Buffalo Grove, IL) and collected on formvar/carbon-coated Ni grids (Electron Microscopy Sciences). The sections on grids were rehydrated with 1 × PBS and then decalcified using 1% ethylenediaminetetraacetic acid (EDTA) solution. After washing with PBS and blocking using 1% ovalbumin (MP Biomedicals, Solon, OH) in PBS for 10 min, grids were incubated in primary polyclonal antibody solutions at 4 °C overnight. Afterward the grids were washed with PBS and blocked again, then treated with a 6 nm-diameter protein A-gold conjugate solution (Electron Microscopy Sciences) for 1 h at room temperature. Sections on grids were washed with Milli-Q water and counterstained with uranyl acetate (Electron Microscopy Sciences) aqueous solution. A JEM 1230 transmission electron microscope (JEOL USA, Inc., Peabody, MA) operated at 120 kV was used to examine the sections.

2.4. Gene expression determined by reverse transcription-quantitative polymerase chain reaction (RT-qPCR) analysis

The TLT was further examined to obtain gene expression levels of TI COL, BSP, OC, OPN, DCN, and VIM with respect to their appearance with animal age (12 and 15 weeks) and as development and mineralization events proceeded in the respective tendons. All tissue segments from the left legs of turkeys preserved frozen in RNA*later* were ground to powders under liquid nitrogen using a cryogenic mill (6870 Freezer/Mill, SPEX SamplePrep, Metuchen, NJ). Total RNA was isolated with TRI reagent following the manufacturer protocol (Molecular Research Center, Inc., Cincinnati, OH). A commercial E.Z.N.A. MicroElute Total RNA Kit (Omega Bio-Tek, Inc., Norcross, GA), was used for column purification of RNA, including a DNase digestion (15 min) using RNase-free DNase (Omega Bio-Tek, Inc.). The quality and quantity of eluted RNA were measured (260/280 ratios) and recorded with an Eppendorf BioPhotometer (Eppendorf, Hauppauge, NY). The corresponding cDNA was synthesized by reverse transcription following a previously reported procedure [54]. Briefly, 1 μg of purified total RNA was reverse-transcribed with the following reaction components: Ambion™ 10 × first strand buffer, dNTPs (2′-deoxynucleoside 5′-triphosphates), random hexamers, oligo (dT) primers, RNase (ribonuclease) inhibitor, and M-MLV (Moloney murine leukemia virus) reverse transcriptase (Invitrogen, Thermo Fisher Scientific, Inc.). Positive control specimens for generation of standard curves in the PCR analysis were prepared in the same manner with isolated RNA from segments of

Table 1
Primer sequences.

Gene	GenBank accession number	Primer	Sequence 5′ to 3′	Product size (bp)	Product melting point (°C)
Bone sialoprotein (BSP)	XM_003205566	F	CTGCATCGCTACAAGGGCA	95	82.5
		R	TGAGTACCTGCATGGGACGG		
Osteocalcin (OC)	XM_003202210	F	AGATCCCAAAGACCCCTCCG	78	77.5
		R	TTCACAAAGGCATGGGCAAC		
Vimentin (VIM)	AY144682	F	GGGTTTGCTTTGCTGTCTGG	54	73.5
		R	CTGGTGTCTGATGAGGCGTT		
Decorin (DCN)	XM_003202126	F	GCTGCCAGTGTCATCTTCGT	82	78.5
		R	GTTGTGTCAGGGGGAAGGTC		

both 12- and 15-week old tendons. Negative controls (minus RT or −RT) were prepared by omitting reverse transcriptase from additional RNA of several different samples.

The primer sets of TI COL and OPN for use in qPCR were initially designed for chicken [37] and then verified for turkey in this study. 18S rRNA served as the standard reference gene, published previously [55]. The primers of other target genes for turkeys were designed using the online Primer-BLAST program from the National Center for Biotechnology Information (www.ncbi.nlm.nih.gov) and then synthesized (Millipore Sigma, Woodlands, TX). Their sequences are listed in Table 1.

PCR was performed on an Applied Biosystems™ 7500 Real Time PCR system (Thermo Fisher Scientific, Inc.) by the relative quantification method [54]. Briefly, in each reaction well of a 96-well plate, the total volume was 20 µl, containing 10 µl of SYBR Green Master Mix, 7 µl of sterile water, 1 µl forward primer, 1 µl reverse primer, and 1 µl cDNA. One or two wells of each plate did not contain cDNA and served as no-template controls (NTC) to verify absence of genomic contamination and formation of primer dimers. Quantitative real-time PCR was run under the following conditions: The plate was annealed at 95 °C for 10 min, then subjected to 40 cycles at 95 °C for 15 s and 60 °C for 30 s (for 18S rRNA) or 60 s (for all other genes). After 40 cycles, a melt curve analysis established amplicon quality and purity. The relative concentrations or quantities of each mRNA in the specimens were obtained according to the standard curve methodology [54,55]. 18S rRNA served as the reference gene in this work because of the small variance of its expression among different experimental samples. All samples were normalized to their corresponding 18S rRNA content from the total RNA isolated from the same turkey tendon sample. Most normalized gene expression data were presented as fold change plots where mineralizing regions were compared to a non-mineralizing portion (calibrator) of the same tendon (See below, Supplemental Fig. 1, and Figs. 3–4).

2.5. Statistical analysis methods

Statistical data analysis (one-way ANOVA) was performed using IBM SPSS Statistics for Windows, Version 20.0 (IBM Corp., Armonk, NY). For one-way ANOVA, the quantities of mRNA were subjected to natural logarithmic transformation to satisfy the assumption of heterogeneity of variance [56]. A Bonferroni post hoc test was performed to compare the statistical difference between the gene expression levels normalized to 18S rRNA of different sample groups. For transformed data possibly violating the heterogeneity of variance assumption, a Games-Howell post hoc test was utilized. Table 2a lists the post hoc test used for each gene. The significance level was set at $p \leq 0.05$. The standard error of the mean (SEM) was used to plot error bars for the corresponding gene expression values. The calculation was $SEM = SD/(N-1)^{0.5}$, where SD is the standard deviation and N is the number of specimens (sample size).

To simplify the ANOVA analysis of sixteen different segments or regions dissected from a given turkey tendon, regions with no statistically significant differences in gene expression were grouped together as one (Fig. 1c). The resulting nine new regions, although different in physical size, were now similar in appearance as unmineralized or partially or heavily mineralized in X-ray evaluation. The relative fold change during gene expression for the various groups was obtained by normalization using the data from the grouped regions 12–16 for both 12- and 15-week-old TLT. The post hoc tests used for the grouped data of each gene are listed in Table 2b.

Table 2a
Post hoc analysis of various genes before grouping.

Sample	12 wk	15 wk R	15 wk L
Gene	Post hoc	Post hoc	Post hoc
TI COL	BF	BF	GH
OPN	BF	BF	GH
BSP	GH	GH	GH
OC	GH	GH	GH
VIM	BF	BF	BF
DCN	BF	BF	BF

BF: Bonferroni; GH: Games-Howell; wk: week; R: the tendon branch inserting into the *M. caput mediale*; L: the tendon branch inserting into the *M. caput caudale*.

Three grouping methods were examined and their mRNA expression levels for different genes are given in Supplemental Fig. 1. A detailed explanation of these grouping methods is given in the legend for Supplemental Fig. 1. Ultimately five regions, segments 1, 2–3, 4–5, 11R, and 12–16R, were chosen for analysis of the 12-week-old turkeys, and nine regions, segments 1, 2–3, 4–5, 6, 7–8, 9–10, 11R, 11L, and 12–16LR, were selected for analysis of the 15-week-old animals. The tendon segments comprising the region 12–16 never mineralized and gave statistically similar expression for various genes. This region was then combined into one group and used as a calibrator (1×). The calibrator (non-mineralizing) was applied to obtain fold changes of gene expression in other regions in various stages of mineralization.

3. Results

An anatomical sketch of the gastrocnemius tendon and the muscles into which it is inserted in a turkey leg is depicted in Fig. 1a. The distal

Table 2b
Post hoc analysis of various genes after grouping.

Sample	12 wk	15 wk R	15 wk L
Gene	Post hoc	Post hoc	Post hoc
TI COL	BF	BF	BF
OPN	BF	BF	BF
BSP	GH	GH	BF
OC	BF	BF	BF
VIM	BF	BF	BF
DCN	BF	BF	BF

BF: Bonferroni; GH: Games-Howell; wk: week; R: the tendon branch inserting into the *M. caput mediale*; L: the tendon branch inserting into the *M. caput caudale*.

aspect of the tissue bifurcates as the tendon passes proximally through a sheath at the leg joint and the divided tendon branches insert into shank muscles of the animal. The tissue immediately proximal to the point of bifurcation is physically thinner than the thicker tissue distal to the tendon division. A normal gastrocnemius tendon from a 15-week-old domestic turkey is depicted in Fig. 1b and c with specific numbered segments or regions of the tendon that were dissected and subjected to gene expression study using RT-qPCR analysis (Fig. 1b). Segments 1 and 6 in the respective right and left bifurcated branches of the gastrocnemius were most proximal in the gastrocnemius examined and segment 16 was most distal (Fig. 1b). Fig. 1c shows tendon regions grouped together for statistical analysis and comparison and described in more detail above (Materials and methods) and below (See Figs. 3–4).

X-ray radiography revealed the mineralized regions in the respective turkey leg tendons (Fig. 2). Radiopaque regions corresponding to the mineralized zones in 15-week-old turkeys are indicated by arrows (Fig. 2b). Mineralization began near the point of bifurcation of the gastrocnemius in these 15-week-old animals, but for individual animals there was variation with respect to the bifurcation in the precise location at which mineralization appeared in each of the tendon branches (Fig. 2b). As determined qualitatively from the X-ray opacity (density) of mineral along the tendon branches, mineralization progressed from distal to proximal regions in each of the branches. Greater opacity was observed nearer the point of tendon bifurcation and less opacity was found in more proximal tendon regions. For each of the 12-week-old turkeys, X-ray images did not show contrast differences near the point of bifurcation or elsewhere in the tendons (Fig. 2a) and mineral was not identified by TEM (data not shown) in these specimens.

Figs. 3 and 4 present X-ray radiographic images and quantitative mRNA expression data for 12-week-old and 15-week-old turkeys, respectively. Certain segments of the tendons were grouped by method I according to similar morphological features as described in Materials and methods and in Supplemental Fig. 1. For each separate or grouped region of the tendons, gene expression data and their standard errors of mean values were obtained and plotted as fold change compared to the calibrator noted previously.

For such gene analysis, five regions were 1, 2–3, 4–5, 11R, and 12–16R for the 12-week-old turkeys. For the 15-week-old turkeys, nine regions were 1, 2–3, 4–5, 6, 7–8, 9–10, 11R, 11L, and 12–16LR. The non-mineralizing zones of these tendons corresponded to the segments or regions 12–16 in either 12-week (Fig. 3) or 15-week (Fig. 4) turkeys.

For 12-week turkeys (Fig. 3a), the two most proximal tendon regions, 1 and 2–3, yielded statistically significantly decreased expression of TI COL compared to distal regions (Fig. 3b). The fold difference of TI COL between proximal and distal areas was on the order of ~40% (Fig. 3b). The two most proximal regions, 1 and 2–3, comprise a transition between the gastrocnemius tendon and the shank muscle, *M. caput mediale* in this case. Although X-ray radiographs did not reveal mineralized regions in this young, 12-week-old turkey leg tendon (Fig. 3a), expression of BSP (expression underlying its depicted fold change as in all Fig. 3b–g) was prominent at branched regions 2–3 and 4–5 near the tendon bifurcation point (Fig. 3c). There was effectively no detectable change in BSP expression in regions 1, 11R and 12–16R and no statistical difference in BSP expression was found among these three regions (Fig. 3c). The same three regions, however, yielded statistically significant ($^*p \leq 0.05$) decreased BSP expression compared to BSP gene expression measured in regions 2–3 and 4–5 (Fig. 3c). The region 4–5 contained the greatest fold change in BSP expression, over 200 times higher than that in the non-mineralizing tendon portion represented by region 12–16R (Fig. 3c). The gene expression pattern of OPN (Fig. 3d) was similar to that for BSP. Tendon regions in the bifurcated branch with regions 1, 2–3, and 4–5 were statistically significantly increased in OPN expression compared to that in regions 11R and 12–16R ($^*p \leq 0.05$), which were effectively absent of such expression (Fig. 3d). More than a 40-fold difference was detected for the regions 2–3 and 4–5 when compared to the non-mineralizing zone, 12–16R (Fig. 3d). No statistically significant difference in OPN expression was noted among the three regions in the bifurcated branch (Fig. 3d). Regarding gene expression of OC, levels were relatively low for regions 2–3, 4–5, 11R and the non-mineralizing zone, 12–16R (Fig. 3e). Region 1 was statistically significantly greater in its OC expression than all other tendon regions and there was an approximately 5-fold increase in the fold change in OC expression levels in region 1 compared to that in region 12–16R (Fig. 3e). The greatest change in gene expression for VIM was in the region 12–16R where it was statistically significantly increased when compared to that in regions 1 and 2–3 ($^*p \leq 0.05$) (Fig. 3f). The fold differences in VIM were about 60% and 40% reduced for regions 1 and 2–3, respectively, when compared to the non-mineralized region 12–16R (Fig. 3f). Gene expression levels in DCN were detectable at relatively low levels over all tendon regions and a statistically significant decrease ($^*p \leq 0.05$) was found on comparing regions 2–3 to region 12–16R (Fig. 3g). These same regions differed by ~40% in their corresponding fold change (Fig. 3g).

For 15-week-old turkeys, each of the two gastrocnemius tendon branches inserting into the muscles of the shank of the animals showed a pattern of mineralization development that proceeded in a distal-to-proximal direction from the tendon bifurcation point (Fig. 4a). As mentioned above, the extreme proximal regions of these tendons typically were more transparent in X-ray radiographic images while distal regions near their bifurcation point were denser and more radiopaque (Fig. 4a). Tendon regions distal to the bifurcation did not mineralize by 15 weeks and were also transparent in X-ray radiograms (Fig. 4a). Because the deposition of mineral was different in location and X-ray opacity in the two proximal tendon branches (Fig. 4a), each of these tissue aspects was analyzed separately for their levels in gene expression and corresponding fold changes of the molecules of interest.

Expression of TI COL was detected in all regions of both proximal tendon branches and there were no statistically significant differences in these gene levels among all these regions of the 15-week-old animals (Fig. 4b, c). The analysis of gene expression of BSP demonstrated statistically significant ($^*p \leq 0.05$) increased levels in mineralizing regions 2–3, 4–5, and 6–11L when compared to levels in the non-mineralizing regions 12–16LR (Fig. 4d, e). Zone 11 is in close proximity to the bifurcation of the tendon into separate, more proximal branches (Fig. 4a). The large standard errors calculated for fold changes for regions 11R and 11L (Fig. 4d, e) indicated BSP gene expression quantities underlying their fold changes were quite variable between the two different proximal tendon branches of the 15-week-old turkey examined. The gene expression of OPN in region 12–16LR was statistically significantly lower than that in all other regions of both tendon branches (Fig. 4f, g). The greatest fold change increase in OPN gene expression, ~70× and 50×, was detected in regions 4–5 and 9–10, respectively, in the two branches when compared to region 12–16LR (Fig. 4f, g). Overall OPN fold changes and underlying gene expression levels (Fig. 4f, g) were approximately correlated with those for BSP (Fig. 4d, e) in that both OPN and BSP fold change and expression values were decreased in regions 1, 6 and 12–16LR compared to all other regions of each tendon branch (Fig. 4f, g). OC fold changes and corresponding gene expression levels did not mimic those of OPN or BSP because both were detected in the non-mineralizing tendon regions 12–16LR (Fig. 4h, i). OC had statistically significantly greater gene expression in tendon regions 2–3 and 7–8 when compared to region 12–16LR with fold change differences of ~4× between these mineralizing and non-mineralizing regions (Fig. 4h, i). Regions 1 and 6 in the two proximal tendon branches also yielded notable OC fold changes and underlying expression levels (Fig. 4h, i). VIM was one of the few genes analyzed that had decreased

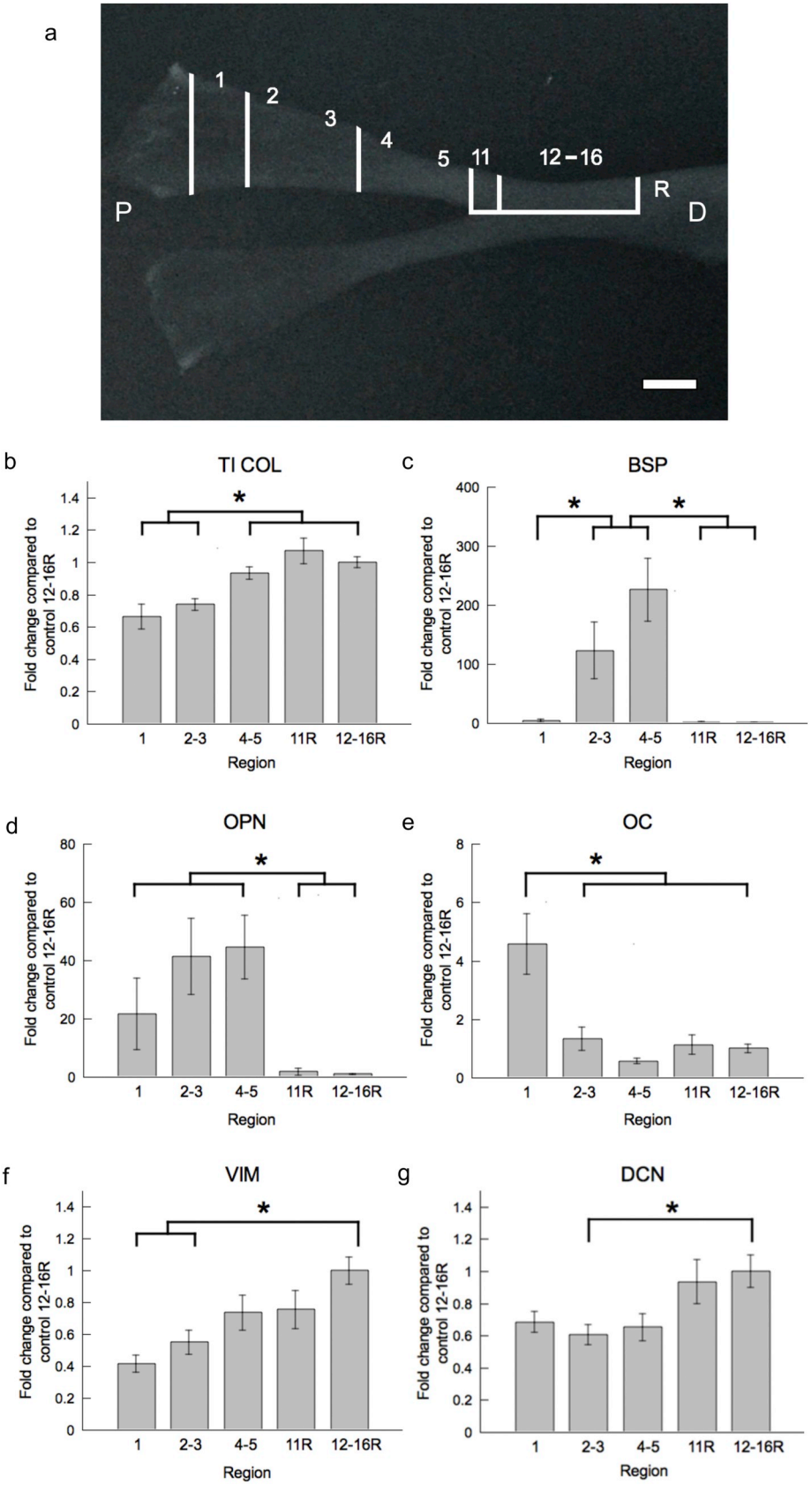

Fig. 3. (a) X-ray radiograph of a 12-week-old turkey leg tendon and its right (R) branch segments grouped and identified according to method I defined in Supplemental Fig. 1. P, proximal; D, distal. Fold change in gene expression was determined for (b) TI COL, (c) BSP, (d) OPN, (e) OC, (f) VIM, and (g) DCN. $N = 7$. While the plots depict fold change, statistically significant differences ($p \leq 0.05$) in corresponding gene expression levels normalized to 18S rRNA between segments or regions of the tendon are denoted by *. The normalizing factor for fold change is segments 12–16R, assigned a value = 1 in all plots. Error bars represent standard error of the mean (SEM) for fold change values. Scale bar: 10 mm.

fold change and expression in mineralizing compared to non-mineralizing regions of 15-week-old tendons (Fig. 4j, k). Regions 1 and 4–5 of the right tendon branch as well as regions 6–10 of the left branch had statistically significantly decreased VIM expression compared to region 12–16LR (Fig. 4j, k). DCN also displayed a trend of decreased fold change values and corresponding gene expression in the mineralizing regions (1 − 10) of both tendon branches when compared to those in non-mineralizing regions (12–16LR) (Fig. 4l, m). A statistically significant decrease in DCN expression levels was measured between regions 9–10 compared to regions 12–16LR in the left tendon branch (Fig. 4m).

Extracellular matrix protein deposition in the gastrocnemius tendon was considered to correspond to gene expression data and it was exemplified by the appearance of collagen and the immunolocalization of BSP and OC (Fig. 5). Collagen fibrils with their characteristic periodic 64–70 nm banding pattern were observed throughout the tissue (Fig. 5a, b) and immunolabeling was found as well for BSP (Fig. 5a, c, d) and OC (Fig. 5b). BSP appeared associated principally with fibrillar aggregates outside collagen fibrils (Fig. 5a) and OC was localized both within and between collagen (Fig. 5b). In representative images of tenocytes, there was immunolabeling of BSP at the level of the Golgi apparatus and rough endoplasmic reticulum (Fig. 5c, d).

Summary changes and comparisons in mineralization and in TI COL, BSP, OPN, OC, VIM and DCN gene expression levels associated with the different regions of the 12- and 15-week-old gastrocnemius tendons from the several turkeys analyzed are presented for two representative specimens. These are the right branches of the tendons from 12- and 15-week-old animals and shown in Figs. 6 and 7,

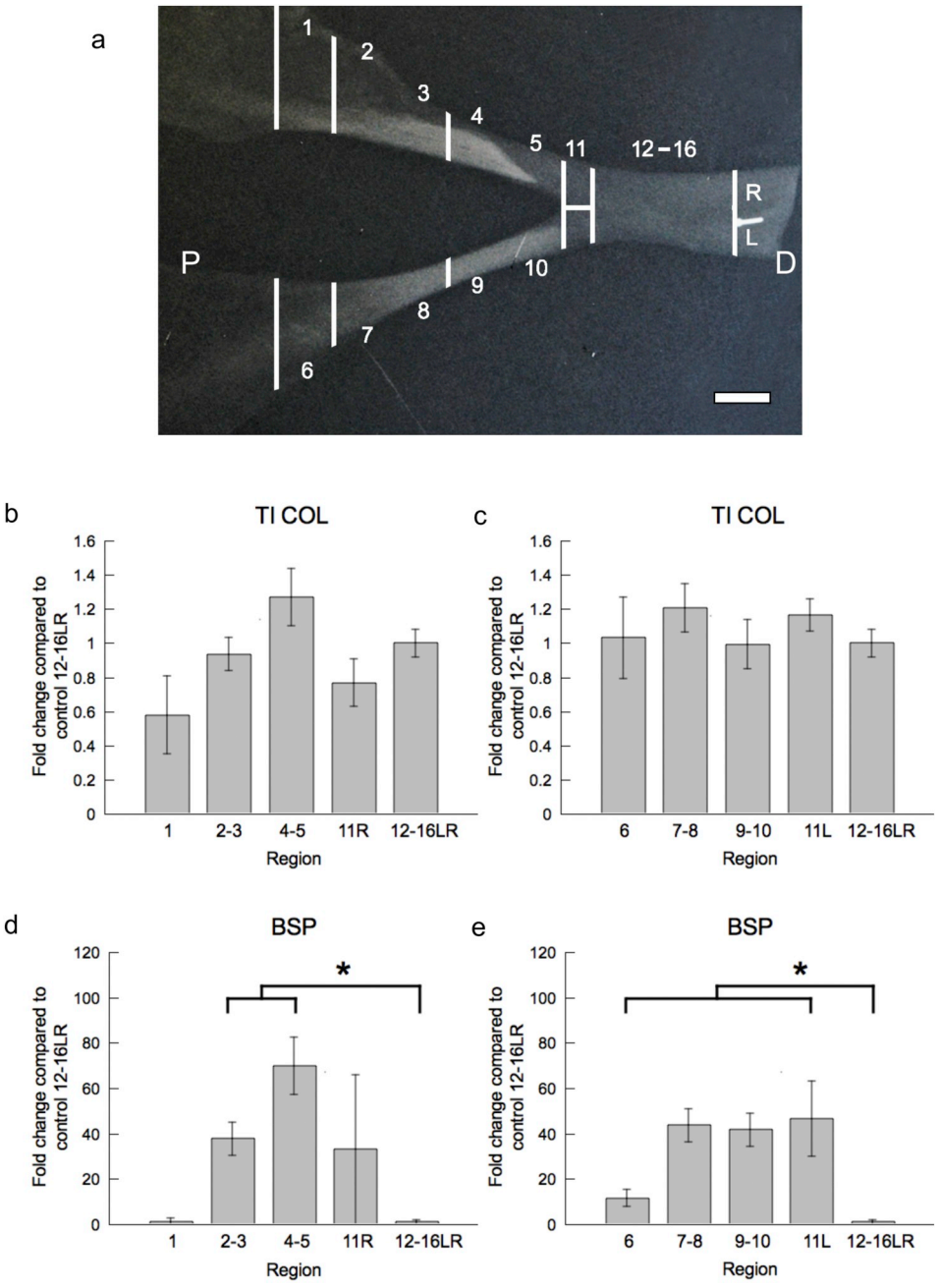

Fig. 4. (*continued*)

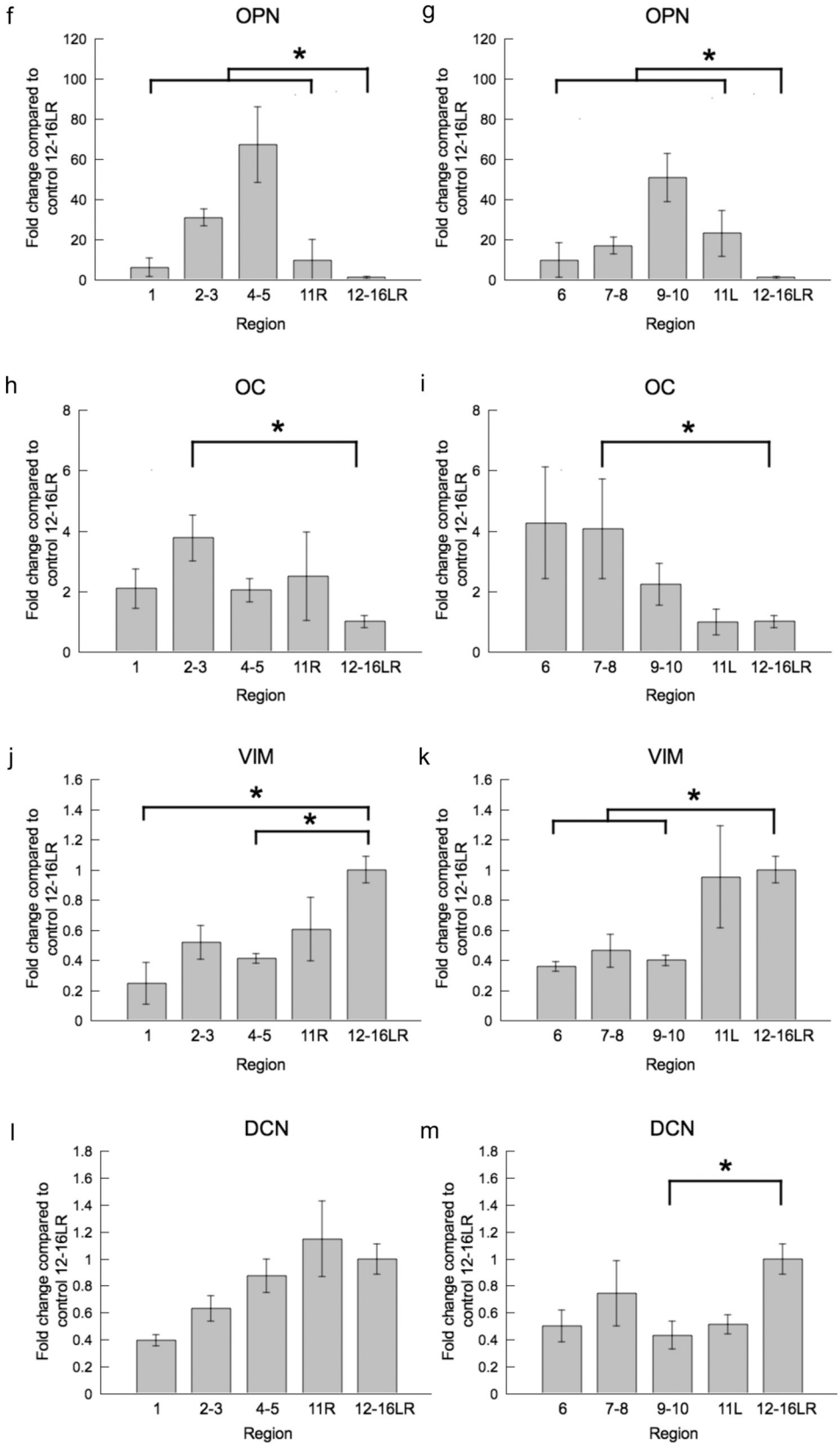

Fig. 4. (a) X-ray radiograph of a 15-week-old turkey leg tendon and its left (L) and right (R) branch segments grouped and identified according to method 1 defined in Supplemental Fig. 1. P, proximal; D, distal. The segments on the R branch inserting into *M. caput mediale* or L branch inserting into *M. caput caudale* of the tendon were each analyzed and compared for fold change in gene expression. Plots of fold change for the R branch are given in (b) TI COL, (d) DCN, (f) BSP, (h) OPN, (j) OC, and (l) VIM while those for the L branch are given in (c) TI COL, (e) DCN, (g) BSP, (i) OPN, (k) OC, and (m) VIM. $N = 3$. While the plots depict fold change, statistically significant differences ($p \leq 0.05$) in corresponding gene expression levels normalized to 18S rRNA between segments or regions of the tendon are denoted by *. The normalizing factor for fold change is segments 12–16R, assigned a value = 1 in all plots. Error bars represent standard error of the mean (SEM) for fold change values. Scale bar: 10 mm.

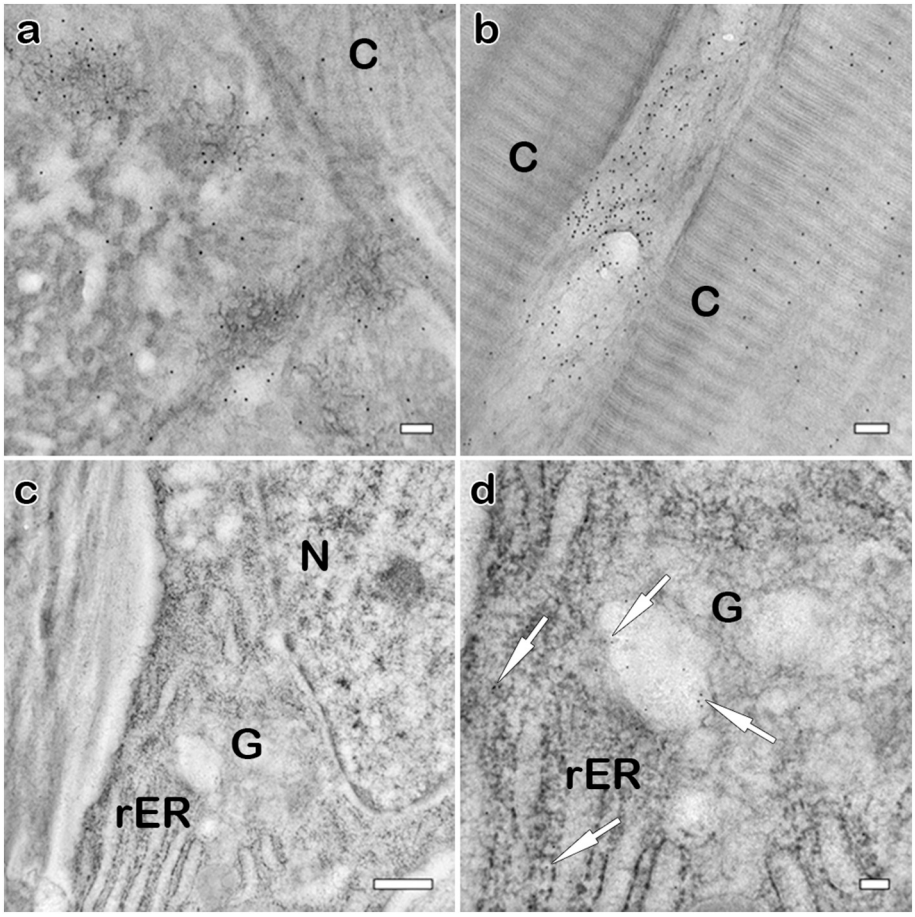

Fig. 5. TEM images of sections of a 15-week-old turkey leg tendon showing immunolocalization of (a) BSP and (b) OC in extracellular tissue regions as well as BSP in tenocyte intracellular regions at (c) low and (d) high magnifications. Sections were subjected to on-grid decalcification with EDTA, immunolabeling, and staining with uranyl acetate [52]. In tendon extracellular spaces, BSP is localized to fibrillar aggregates close to collagen fibrils (a). Immunolabeling of OC is associated with extracellular spaces both inside and outside collagen (intrafibrillar and interfibrillar collagen, respectively; b). Typical ultrastructural features of tenocytes have been preserved during the immunocytochemical procedures and nuclei (N), rough endoplasmic reticulum (rER), and the Golgi apparatus (G) of tendon cells can be identified at low magnification (c). In this study, the gold nanoparticles for immunolabeling were very small (diameter ~6 nm) and they were better resolved at relatively higher magnification (d, enlargement of c). BSP labeling (arrows) is mainly associated with rER and the vacuoles of G (d). Collagen (C). Scale bar: (a) 100 nm, (b) 100 nm, (c) 500 nm, and (d) 200 nm.

respectively, together with Fig. 8a and b, depicting the gene expression levels correlated with the X-ray radiographs of the tendons. Here the tendon regions were ungrouped and expression of genes relative to each other was determined in each tendon for the eleven evenly divided segments, 1–5 and 11R–16R, comprising either the 12- or 15-week-old tendons examined as also shown in Fig. 1b or Fig. 2b, respectively. The expression levels normalized to 18S rRNA are plotted in Figs. 6 and 7 as distinct from the fold changes in gene expression given in Figs. 3 and 4 for same-aged tendons. In the 12-week tendon specimen (Fig. 6a), the tissue region distal to the point of bifurcation (segments 11R–16R), compared to the region more proximal (segments 1–5), appeared approximately the same or was relatively lower in expression of the genes analyzed except for VIM (Fig. 6f) and perhaps TI COL (Fig. 6b) and DCN (Fig. 6g). VIM expression levels generally increased with increasing distal distance from the point of bifurcation (Figs. 6f, 8a). In the regions proximal and close to the bifurcation point (segments 3–5), BSP expression was relatively high compared to that of the other genes (Figs. 6c, 8a). In the most proximal regions of the tissue branch distant from its bifurcation point (segments 1–2), OC expression was relatively highest compared to all other genes (Figs. 6e, 8a).

In the 15-week tendon specimen, where mineralization had occurred in its right segments 2–5 and left segments 7–10 (Fig. 7a), the normalized expression profiles for all respective genes resembled one another in both tendon branches (Fig. 7b–m). Fig. 8b presents the relative expression values of the genes analyzed in the right branch corresponding spatially to the tendon itself. For either tendon branch, the region of the gastrocnemius distal to its bifurcation point (segments 12–16) yielded little or no expression of BSP (Figs. 7d, e and 8b) or OPN (Figs. 7f, g and 8b). This region was relatively lower in expression of all genes except for VIM (Fig. 7j, k), which, like that in the 12-week specimen examined (Fig. 6f), was found to have relatively higher expression levels that also appeared to increase with increasing distal distance from the tendon point of bifurcation. In the regions proximal and close to the point of bifurcation (segments 3–5 and 8–10), both BSP (Fig. 7d, e) and OPN (Fig. 7f, g) gene expression was notably elevated compared to that of all other genes although OC (Fig. 7h, i) was modestly high. Segments 2 and 7 were also relatively high in BSP (Fig. 7d, e) and OPN (Fig. 7f, g) gene expression. In the most proximal tendon aspects distant from the bifurcation point (segments 1–2 and 6–7), OC was greater in its expression compared to all other genes accessed; it was also high in segments 3 and 8 (Fig. 7h, i).

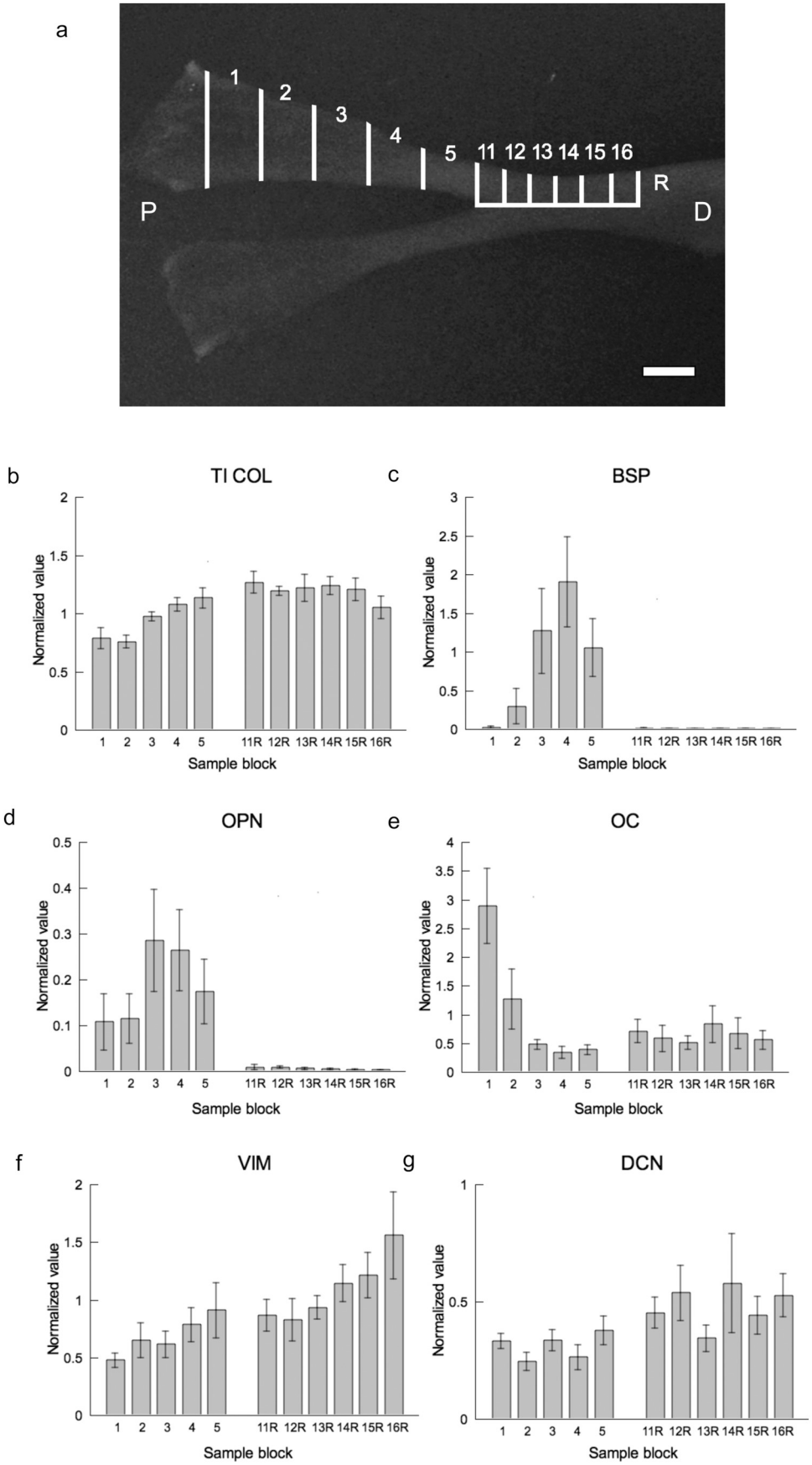

Fig. 6. (a) X-ray radiograph of the 12-week-old turkey leg tendon shown in Fig. 3 and its individual right (R) branch segments identified without grouping. P, proximal; D, distal. Gene expression levels normalized to 18S rRNA were determined for (b) TI COL, (c) BSP, (d) OPN, (e) OC, (f) VIM, and (g) DCN. $N = 7$. Error bars represent standard error of the mean (SEM) for normalized gene expression values. Expression values are plotted against corresponding segments in Fig. 8a. Scale bar: 10 mm.

Certain trends in gene expression were observed on comparison with the mineralized and non-mineralized morphological regions visualized radiographically from the avian tendons (Fig. 8a, b). TI COL expression appeared consistent over all regions of both the 12- and 15-week-old tendons analyzed. BSP expression levels rose and then fell in the tendon regions that were to be mineralized in the 12-week-old tendon and before the presence of mineral was detected by X-ray radiography in 15-week-old specimens. OC levels were highly elevated in regions that inserted or were close to the shank muscle of the 12-week-old tendon. In the 15-week-old tendon, OPN, BSP and OC levels were each elevated and all rose and fell over proximal-to-distal tissue regions as mineralization correspondingly progressed toward the tendon point of bifurcation. VIM was found to follow a pattern of rising in expression from proximal-to-distal aspects of the tendon; its greater expression values occurred at the extreme distal end of tendon analysis, and opposite to the pattern of OC, which yielded greater values at the extreme proximal regions of the same tendon. On comparing expression of like genes in 12- and 15-week-old tendons, levels of OPN, BSP, and OC markedly increased over the regions proximal to the point of bifurcation in the mineralizing, older tissues while TI COL decreased throughout the full length of the same 15-week-old tissues examined.

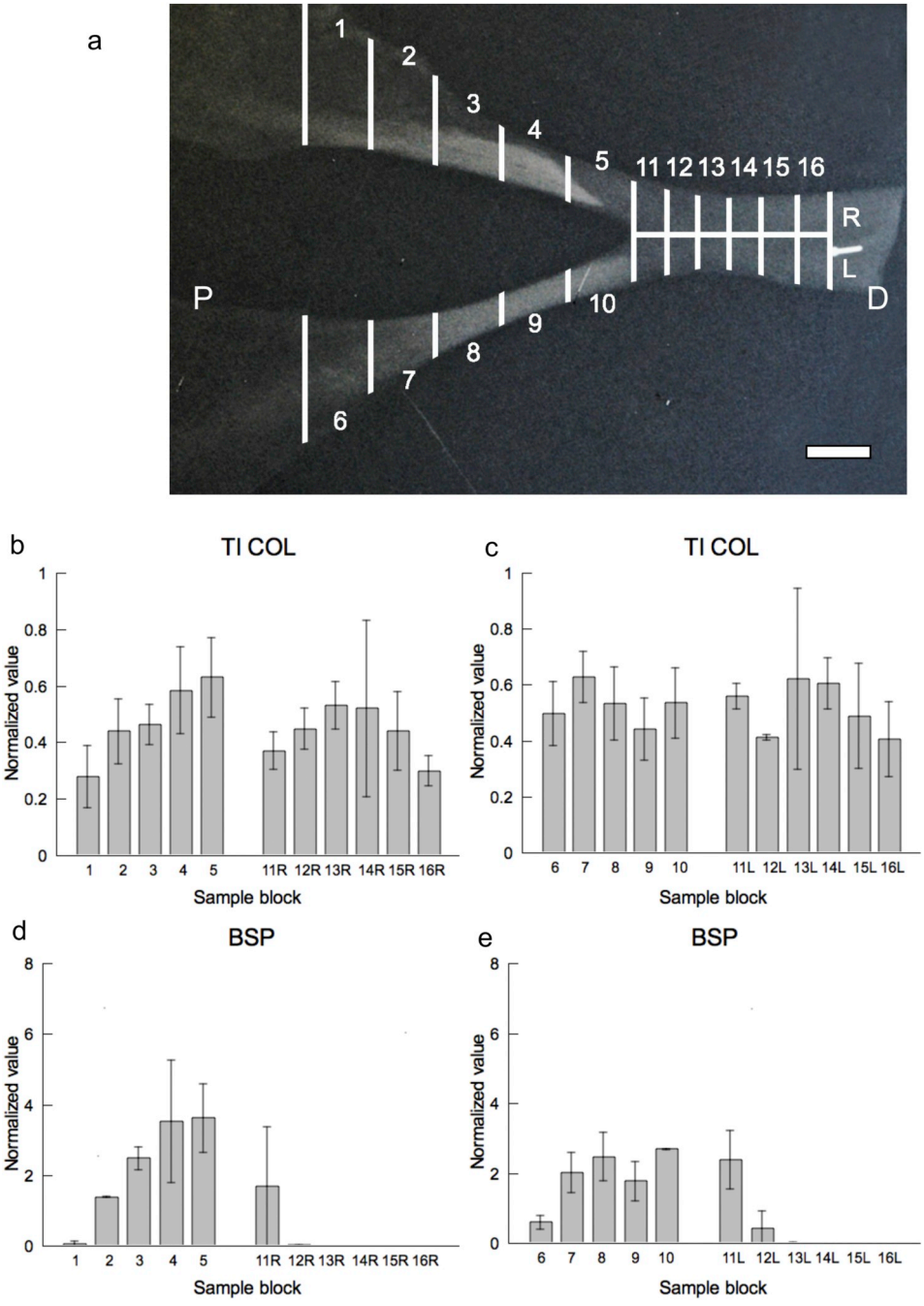

Fig. 7. (*continued*)

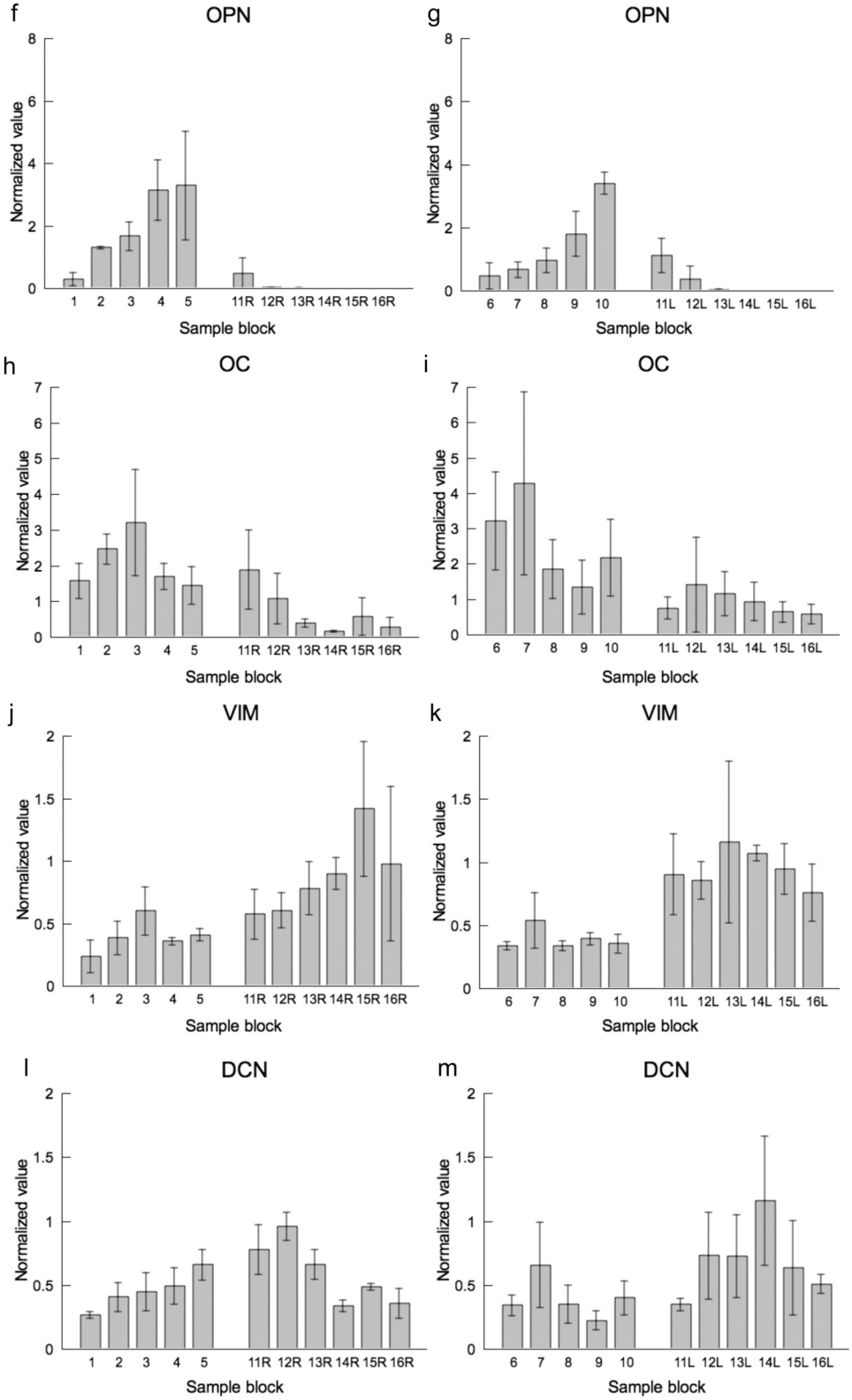

Fig. 7. (a) X-ray radiograph of the 15-week-old turkey leg tendon shown in Fig. 4 and its individual right (R) and left (L) branch segments identified without grouping. P, proximal; D, distal. Gene expression values normalized to 18S rRNA were determined and plotted for the right tendon branch in (b) TI COL, (d) BSP, (f) OPN, (h) OC, (j) VIM, and (l) DCN and for the left branch in (c) TI COL, (e) BSP, (g) OPN, (i) OC, (k) VIM and (m) DCN. Statistical significance was determined as $p \leq 0.05$ (*). $N = 3$. Error bars represent standard error of the mean (SEM) for normalized gene expression values. Expression values are plotted against corresponding segments in Fig. 8b. Scale bar: 10 mm.

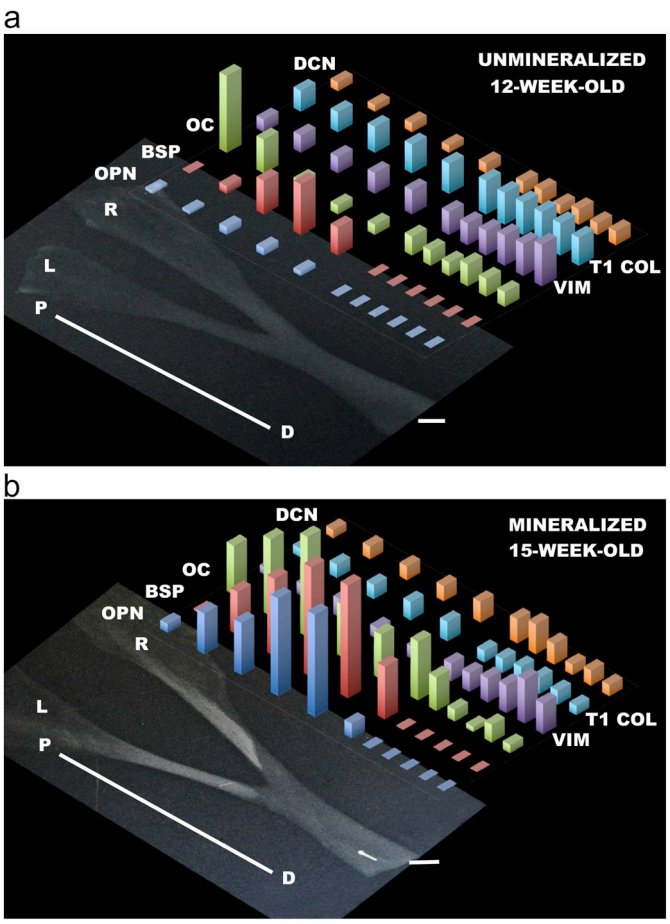

Fig. 8. Diagram correlating gene expression levels for OPN, BSP, OC, VIM, TI COL and DCN (Figs. 6, 7) with the segmental sites along the right (R) branch of the tendons from a (a) 12-week-old and (b) 15-week-old turkey imaged by X-ray radiography (Figs. 6 and 7, respectively). The expression levels of the individual genes of interest are clearly shown spatially and relative to one another in the younger, unmineralized and older, mineralized tendon specimens. L, left tendon branch; P, proximal; D, distal. A few of the findings include, for the 12-week-old tendon, the observations that BSP expression prominently rises and falls along the proximal tendon region destined to mineralize at a later time; OC expression is greater in proximal tendon regions close to the muscle insertion site at the shank; OPN and BSP expression is minimal in regions distal to the point of tendon bifurcation while VIM expression increases along the same distal portions of the tissue; and TI COL and DCN expression is relatively constant over the full extent of the tendon examined. For the 15-week-old-specimen, OPN, BSP, and OC expression each rises and falls somewhat synchronously through the mineralized proximal aspect of the tissue; the same genes are expressed at minimal levels over much of the tendon aspects distal to the point of bifurcation; VIM expression is lower in tendon regions proximal to the bifurcation point of the tissue and increasingly greater distal to the point, a pattern of expression opposite to that of OC; and TI COL and DCN expression is relatively constant over the full tendon length investigated. Scale bars: 10 mm.

4. Discussion

The mineralization of vertebrate tissues in vivo occurs through a series of highly interrelated and coordinated spatial and temporal events. The development and formation of mineral in these tissues may be elaborated in part by examining the sequence of expression of genes and the synthesis and secretion of their proteins or other molecules in the tissues. Studies in vitro with cultures of osteoblasts [36,37] and stem cells [58] as well as work in vivo with embryos [28], fetuses and neonates [30], for example, suggest that cell differentiation, gene expression and corresponding matrix molecule deposition, and mineralization follow in the carefully regulated manner noted above. As a result of these and additional investigations, some of the proteins, such as BSP, are thought to be correlated with cell differentiation and initial mineral formation while others, such as OC, appear to be involved in matrix maturation [30,58–60]. Effects of additional genes, proteins and molecules on differentiation and mineralization have been reported [61–63].

The study presented here clearly demonstrates that certain aspects of the morphological appearance and biochemistry of turkey leg tendons resemble those of bone. Gene analysis and immunolocalization document respectively the expression and presence of several NCPs, including OPN, BSP, and OC, in the tendons as they are in bone. Indeed, OC expression levels are notably greatest in tendon regions in the vicinity of their muscle insertion sites, a result reported here for the first time. This work also provides understanding about whether these NCPs occur simply through their deposition from blood vessels [43] or as the products of local tendon cells. Again, gene expression and immunocytochemistry of individual tendon segments and their constituent tenocytes show that these cells themselves are actively involved in the processing, synthesis and secretion of NCPs in the progressive structural and temporal development of both unmineralized and mineralized tendons.

With regard more specifically to turkey gastrocnemius tendon development and its subsequent mineralization, the distribution of mineral follows a spatial and temporal pattern in which the earliest deposition is more proximal in the bifurcated tendon branches and the most mature deposition is distal to the tissue, near the tendon bifurcation point [27]. The animals must reach a certain age before mineralization first becomes apparent in the gastrocnemius (as detected by X-ray means, for example), and in this work they must be older than 12 weeks and likely at least 13 weeks of age. Thus, regarding location and at the appropriate time of development of the birds and their leg tendons, mineralization begins in the vicinity of the gastrocnemius bifurcation and then progresses in a proximal direction along the tendon branches as further growth and aging occur [27]. Such mineral deposition and structural development of the gastrocnemius tendon with animal age are expected to be associated with various extracellular matrix proteins and their particular distributions, which can be correlated with the corresponding gene expression measurable using RT-qPCR as done in this investigation. It can be noted that the onset of mineralization at the gastrocnemius branch point may be the consequence of greater stress or strain levels in the tendon as it undergoes a change at this location from a single wider diameter structure distally to two narrower diameter branches more proximally [27]. Each gastrocnemius tendon examined in this study begins to mineralize in its region of bifurcation, but there are differences in mineralization that can be detected from one tendon to another by X-ray radiography. For instance, some tendons exhibit wedged-shaped, tapered mineral deposition while others have blunted edges of mineralization. Some tendons may also begin to mineralize at different locations and distances proximal to the exact point of bifurcation. These variations can be observed in the regions or segments of the tendons identified as 4–5 and 9–10 in this study. Such observations are consistent on comparison with published literature [27].

The deposition of type I collagen is a principal event in vertebrate mineralization. In general, type I collagen is one of the first extracellular proteins to be secreted by vertebrate tissue cells, including tenocytes. Type I collagen provides the proper environment and signaling cues to the cells to prompt further secretion of other molecules to enhance extracellular matrix and mineral formation. Studies in vitro suggest that collagen expression decreases after the onset of mineralization [63,64], and comparison in the work here in vivo between collagen expression levels from unmineralized 12- and mineralized 15-week-old tendons supports this statement. Further in the leg tendons presently investigated, type I collagen gene expression is detected along

all such tissues at either 12 or 15 weeks of development. There was a trend found toward increasing expression of type I collagen along the proximal-to-distal direction of a yet unmineralized, 12-week gastrocnemius tissue branch, but no statistically significant differences in the expression of this gene were observed among the different regions of the tissue retrieved by 15 weeks and after mineralization had begun. As noted above, the gastrocnemius tendons at these two time periods are physically thinner proximally from their point of bifurcation compared to their distal regions, but each of these proximal aspects of the tissue is characterized by gene expression and secretion of type I collagen adequate to support not only mineral formation but also the proper insertion of the tendon into its neighboring shank muscle. This latter result is given evidence from the gene expression and microscopic data from regions 1 and 2–3 in the tendons reported in the present study. Thus, type I collagen is a crucial matrix protein in both the mineralized and unmineralized aspects of gastrocnemius tendon tissues.

Several roles for BSP in vertebrate mineralization have been discussed in an earlier review [65]. Studies suggest that BSP is an effective nucleating agent for hydroxyapatite [2,66–68] as well as a determinant for osteoblast differentiation [59,60]. The gene expression of BSP appears to be a possible marker for the onset of mineralization [30,58]. The gastrocnemius regions 4–5 and 9–10 for both the younger and older turkeys investigated here yield the highest BSP expression in these tissues. These regions are most heavily mineralized in the 15-week-old tendons and both regions, despite the fact that mineral cannot be detected by radiography in the 12-week animals, are destined to mineralize first in the vicinity of the point of bifurcation in those tendons. Such coincidence in BSP expression and tendon location clearly suggests that BSP is important in regulating the gastrocnemius mineralization process especially prior to and during initial stages of apatite deposition. This conclusion is consistent with those of previous reports [35,69].

The Arg-Gly-Asp (RGD) motif in its backbone suggests a role for BSP in regulating cell behavior [34], and BSP is reported to promote osteoblast differentiation in vitro [59,60]. In the study here, the overall higher expression of BSP in both unmineralized and mineralized branched regions of the turkey leg tendon may indicate BSP involvement in tenocyte differentiation to an osteoblast-like phenotype in expressing additional genes and secreting additional molecules necessary for mineralizing the gastrocnemius tendon. The deposition of BSP by tenocytes is evidenced by its immunolocalization associated with rER and vacuoles of the Golgi apparatus, results suggesting active synthesis and secretion of BSP by these cells. Further, immunolocalization of BSP appears in association with type I collagen fibrils, more specifically, with extracellular matrix sites along or on the surfaces of type I collagen or outside and beyond neighboring collagen fibrils. These ultrastructural features of BSP resemble those in a recent immunocytochemical study of BSP and OC in mineralizing turkey leg tendon [52] as well as in other reports concerning osteoblasts [12,18,69–71].

The possible functions of OPN with respect to mineralized tissues have been discussed earlier by other research groups [16,72,73]. Like BSP, OPN also contains an RGD motif and is involved in regulation of cell behavior, such as promoting cell adhesion on a bone surface. It is notable that OPN is a matrix protein not specific to mineralized tissues [73,74], and it may inhibit mineralization and control apatite crystal growth [75,76]. In this study, the expression of OPN in the gastrocnemius tendons shares some features with BSP in their common appearance and pattern of fold changes in certain of the tissue regions. Fold changes in 12-week-old tendons, for example, rise simultaneously and markedly for both OPN and BSP toward the bifurcation point in proximal unmineralized tissue regions and both OPN and BSP are minimally detected in regions distal to the point. In 15-week-old tendons, fold changes in OPN and BSP increase again in proximal mineralized tissue aspects and toward the point of bifurcation and the fold changes remain minimally detectable distal to the point. Gene expression, itself, for both molecules follows a similar pattern in either 12- or 15-week-old tendon specimens examined. There are also examples of differences between OPN and BSP: For 12-week-old turkeys, relative fold changes in OPN and BSP expression are found to be quantitatively varying, ~40 and > 200, respectively, in tendon regions closest to the point of bifurcation where mineralization will begin proximally in the tissue, and, for 15-week-old turkeys, ~50–70 and ~40–70, respectively, in the same regions closest to the bifurcation point and where mineralization has already begun by this time in tendon maturation. These data indicate that expression of both OPN and BSP is upregulated before the onset of mineralization in the tendon, although to different degrees, and that each molecule is involved in early as well as later stages of mineral deposition in this tissue. The results in expression of these two NCPs likely underlie their different functions in regulation of cell behavior and mineralization events, and such a conclusion is consistent with that presented in previous studies [28,30].

Following reports based on other mineralized tissue models, OPN is associated with osteoblast differentiation and bone formation. Its mass appears to increase with mineral accumulation at early stages of matrix mineralization [64], and OPN has been suggested to bind to pre-existing apatite crystals to regulate their growth [16]. Increasing mineral formation is anticipated to be accompanied by additional OPN deposition, a result that may be correlated with increased OPN expression and the spatial mineral distribution observed in mineralized regions of the older, 15-week leg tendons.

OC is a vitamin K- and D-dependent NCP secreted by mineral-forming cells [77] such as osteoblasts [78–80] and odontoblasts [14,70,81]. Other non-mineral-forming cells such as fibroblasts do not typically synthesize OC [82]. OC mRNA is generally expressed at later stages of osteoblast differentiation that accompany mineral deposition [64,83]. Accumulation of OC has also been found in pathological mineralization such as urolithiasis [84]. While previous studies of the OC gene knock-out model [25,26] and work in vitro [3] have shown that OC inhibits mineral formation or delays apatite nucleation, other investigations demonstrate that OC can facilitate apatite formation through a dissolution-reprecipitation process [85]. OC may as well form a complex with OPN that promotes apatite nucleation [7]. These various reports support a role that, like BSP [2,11,17,34,35,65–68,86–90], OC is involved in aspects of the dynamic process of mineralization [5,12,14,52,70,71,77,81,84,85,91–95].

The changing content of circulating OC in serum has been correlated with several bone diseases [96]. Current work suggests that the functions of OC vary with its different structural forms: The carboxylated form of OC is associated with mineralization [77]. The undercarboxylated OC acts as a hormone for regulation of glucose metabolism, insulin secretion, male fertility, and brain development [1,97–99]. From the present work, mineralized turkey leg tendon yields both gene expression and immunolocalization of OC. The spatial distribution of OC gene expression shows distinctive patterns along the tendon at different ages of the animals and especially in mineralizing regions (such as tendon segments 2–3 and 7–8). For younger, 12-week-old turkeys, the very proximal tendon (segment 1) has markedly higher levels of expression of OC and such levels, while remaining relatively elevated, appear somewhat diminished in the same segment of older, 15-week turkeys. The observed higher levels of OC in the most proximal tendon regions of younger birds are interesting and may be related to possible OC presence in muscle. The latter supposition is based on reports that OC mediates skeletal muscle strength [100] and vascular smooth muscle [101].

Compared to segment 1, expression of OC increases in more mineralized tendon regions proximal to the point of bifurcation in 15-week-old birds. Deposition of OC may precede mineralization [102,103], and more recent work in which decalcification of tendon is found to enhance OC detection by immunocytochemical methods suggests a close association in time and location between OC deposition

and mineralization [52]. In this immunolabeling study, the addition of Ca^{2+} during immunolocalization indicated the carboxylated form of OC being labeled in mineralizing gastrocnemius tendon, and OC was proposed to mediate both intra- and interfibrillar collagen mineralization in this tissue [52]. The unmineralized regions of tendons (12–16LR) in this report also yield detectable, although low, levels of OC expression, a result again suggesting that OC mRNA is present in these as well as mineralized tendon aspects.

An intriguing implication of the observed upregulation of OC expression in both unmineralized and mineralized tendons reported here is that, assuming secretion of the protein follows its expression in a normal manner, OC would likely be associated with type I collagen during collagen fibril assemblage. If so, OC would potentially be located in the hole zone regions of the fibrils and along collagen surfaces, as found by immunocytochemistry [52], already in place possibly to modulate later and impending events of nucleation, growth and/or development of apatite crystals at those intra- and interfibrillar collagen sites [52].

On the other hand, an association of this nature between OC and collagen formation may be reflective of the recognized capacity of mineralized collagenous tissues and mineral in particular to serve as a storage reservoir for small molecules and a variety of anions and cations [104,105]. Correlation of OC expression with collagen and mineralization documented in the present study and OC immunolocalization to specific sites within and along collagen fibrils in mineralizing avian tendon [52] may be indicative of OC binding in tissues that may undergo subsequent remodeling and release of the molecule to the circulation. In this context, rather than putatively being involved in mediating apatite crystal nucleation, growth, and/or development, OC may be sequestered in an inactive state within or on collagen, thereafter functioning as a hormone on its entry into the circulation [1,97–101]. Resolution of these alternative actions of OC awaits further investigation.

VIM and OC expression appears to be inversely related in the present work. VIM can affect the transcription of OC by inhibiting the transactivation activity of ATF4 [106,107]. Although the fold differences are relatively small, the gastrocnemius tendons from the turkeys that were either 12- or 15-weeks-old gave similar information that VIM expression is greater while OC expression is lower in unmineralized tissue regions (12–16R or 12–16LR). This result is consistent with reports correlating VIM and OC [106,107] as well as OC and mineralization, that is, VIM may serve to inhibit OC expression and subsequent protein synthesis and secretion.

VIM is a cytoskeletal component regulating intracellular mechanics [108,109]. The VIM intermediate filament facilitates the transmission of a mechanical signal from the extracellular matrix to the cell and regulates cell behavior in response to shear stress [110]. Therefore, cytoskeletal components such as VIM possibly regulate gene expression of other NCPs such as OC and resulting extracellular mineralization through a mechanism in response to external stresses in tendon exerted by the muscles into which tendon tissues insert. Several reports have shown that external forces can affect the gene expression of osteoblasts [111–114]. However, the corresponding expression of VIM does not show a significant change [113,115]. Further studies in osteoblasts and tenocytes are needed to elucidate possible relations between stress, VIM, OC and cytoskeletal elements that may regulate their respective cell behavior as well as their consequent extracellular matrix production and mineralization.

Proteoglycan content is reported to vary with mineralization in turkey tendon [20]. In this context, DCN belongs to the small leucine-rich proteoglycan (SLRP) family and binds to type I collagen on d and e bands in its gap region [116]. Immunolocalization studies suggest that DCN affects mineralization [117]. In the current study, the expression of DCN by tenocytes in the gastrocnemius in both 12- and 15-week-old turkeys yields significantly lower expression levels in mineralizing compared to non-mineralizing tendon regions. This observation may be a reflection of the fact that non-mineralizing aspects of these tendons may be replete with proteoglycans but mineralizing regions require fewer of these molecules and more available matrix space in order for mineralization to proceed. Tenocytes, then, in the mineralizing tendon regions are less active in their gene expression and subsequent synthesis of DCN and related proteoglycan molecules. In this regard, there may be proteoglycan degradation by metalloproteinases [118] during tendon development and mineralization. Degradation of proteoglycans may release ions available for mineral formation. If proteoglycans are bound to type I collagen surfaces, degradation may also provide open spaces on or along the surface hole regions of the collagen fibrils, facilitate diffusion of small NCPs (such as OC; [52]), and enhance nucleation of apatite crystals in intra- and interfibrillar collagen molecules comprising the tissue. Further studies will be necessary to gain insight into these possibilities.

As an added note, this study was principally concerned with a comparison between the spatial and temporal pattern of normal TLT mineralization and the expression in the tissue of certain genes and the secretion of their counterpart extracellular matrix molecules. In the present work, an exact relation is unclear between the levels of gene expression and the levels of secretion of the molecules corresponding to those genes. A detailed proteomics analysis correlated with gene expression measures and tendon structure and mineralization is currently being assessed in this laboratory to establish expression-secretion levels more precisely.

Finally, from a clinical translational point of view, the avian leg tendon model provides a fundamental basis for understanding how normal vertebrate mineral deposition occurs in relation to the expression of certain genes and their secreted molecule counterparts. Ectopic mineralization and other pathologies of mineral deposition that occur in human tendon or additional tissues such as bone, dentin and cementum may then be compared with the mineralizing avian tendon through precise biochemical (compositional) and physical (structural) parameters as a possible means of gaining insight into or determining the underlying cause(s) of such abnormalities.

5. Conclusion

In summary, this study correlates gene expression levels of several NCPs and other molecules with the temporal and spatial development of mineral in the avian leg tendon. The expression by tenocytes of TI COL, BSP, OPN, OC, VIM, and DCN varies depending on time (age) of tendon and turkey development and location within or along the gastrocnemius tendon. BSP expression appears to be a marker for mineral formation in the tendons as it is found in gastrocnemius regions that are destined to become mineralized as well as those regions in which mineral deposition is actively occurring and has already occurred. OPN expression generally follows that of BSP although OPN is considered inhibitory to mineral formation. OC expression is present at moderate levels in tendon regions to be mineralized and it is also found at greater levels where mineralization is observed. The onset and pattern of its expression imply that OC is present as collagen fibrils assemble and the protein is in place associated with collagen prior to its possible action as a mediator of mineral nucleation and subsequent events of apatite crystal growth and development or as a hormone released to the circulation following tissue remodeling. VIM expression appears inverse to that of OC, that is, higher in non-mineralizing tendon regions and lower in aspects of the tissue undergoing mineralization. VIM may serve to inhibit OC expression in the tissue and VIM may be regulated itself by biomechanical factors affecting the tendons with time of development and tendon location. Expression of DCN mRNA seems unaffected by tendon mineralization and the actual content of DCN may be regulated by metalloproteinases and proteoglycan degradation in the tissue. Immunolocalization of BSP and OC identifies these protein products of their respective genes and demonstrates a structural association between BSP and interfibrillar collagen and between OC and both

interfibrillar and intrafibrillar collagen.

Supplementary data to this article can be found online at https://doi.org/10.1016/j.bone.2018.11.005.

References

[1] G. Karsenty, M. Ferron, The contribution of bone to whole-organism physiology, Nature 481 (2012) 314–320.
[2] G.K. Hunter, H.A. Goldberg, Nucleation of hydroxyapatite by bone sialoprotein, Proc. Natl. Acad. Sci. U. S. A. 90 (1993) 8562–8565.
[3] G.K. Hunter, P.V. Hauschka, A.R. Poole, L.C. Rosenberg, H.A. Goldberg, Nucleation and inhibition of hydroxyapatite formation by mineralized tissue proteins, Biochem. J. 317 (1996) 59–64.
[4] P.V. Hauschka, S.A. Carr, Calcium-dependent alpha-helical structure in osteocalcin, Biochemistry 21 (1982) 2538–2547.
[5] P.V. Hauschka, F.H. Wians, Osteocalcin–hydroxyapatite interaction in the extracellular organic matrix of bone, Anat. Rec. 224 (1989) 180–188.
[6] N.M. Ritter, M.C. Farach-Carson, W.T. Butler, Evidence for the formation of a complex between osteopontin and osteocalcin, J. Bone Miner. Res. 7 (1992) 877–885.
[7] A. Gericke, C. Qin, L. Spevak, Y. Fujimoto, W.T. Butler, E.S. Sørensen, A.L. Boskey, Importance of phosphorylation for osteopontin regulation of biomineralization, Calcif. Tissue Int. 77 (2005) 45–54.
[8] Y. Wang, T. Azaïs, M. Robin, A. Vallée, C. Catania, P. Legriel, G. Pehau-Arnaudet, F. Babonneau, M.-M. Giraud-Guille, N. Nassif, The predominant role of collagen in the nucleation, growth, structure and orientation of bone apatite, Nat. Mater. 11 (2012) 724–733.
[9] H.A. Goldberg, K.J. Warner, M.J. Stillman, G.K. Hunter, Determination of the hydroxyapatite-nucleating region of bone sialoprotein, Connect. Tissue Res. 35 (1996) 385–392.
[10] M.D. McKee, A. Nanci, Postembedding colloidal-gold immunocytochemistry of noncollagenous extracellular matrix proteins in mineralized tissues, Microsc. Res. Tech. 31 (1995) 44–62.
[11] P. Bianco, M. Riminucci, G. Silvestrini, E. Bonucci, J.D. Termine, L.W. Fisher, P.G. Robey, Localization of bone sialoprotein (BSP) to Golgi and post-Golgi secretory structures in osteoblasts and to discrete sites in early bone matrix, J. Histochem. Cytochem. 41 (1993) 193–203.
[12] M.D. McKee, M.C. Farach-Carson, W.T. Butler, P.V. Hauschka, A. Nanci, Ultrastructural immunolocalization of noncollagenous (osteopontin and osteocalcin) and plasma (albumin and alpha 2HS-glycoprotein) proteins in rat bone, J. Bone Miner. Res. 8 (1993) 485–496.
[13] P. Bianco, Y. Hayashi, G. Silvestrini, J.D. Termine, E. Bonucci, Osteonectin and Gla-protein in calf bone: ultrastructural immunohistochemical localization using the protein A-gold method, Calcifi. Tissue Int. 37 (1985) 684–686.
[14] I. Gorter De Vries, D. Coomans, E. Wisse, Ultrastructural localization of osteocalcin in rat tooth germs by immunogold staining, Histochemistry 89 (1988) 509–514.
[15] A.A. Poundarik, T. Diab, G.E. Sroga, A. Ural, A.L. Boskey, C.M. Gundberg, D. Vashishth, Dilatational band formation in bone, Proc. Natl. Acad. Sci. U. S. A. 109 (2012) 19178–19183.
[16] M.D. McKee, A. Nanci, Osteopontin and the bone remodeling sequence - colloidal-gold immunocytochemistry of an interfacial extracellular matrix protein, Ann. N. Y. Acad. Sci. 760 (1995) 177–189.
[17] J. Chen, M.D. McKee, A. Nanci, J. Sodek, Bone sialoprotein mRNA expression and ultrastructural localization in fetal porcine calvarial bone: comparisons with osteopontin, Histochem. J. 26 (1994) 67–78.
[18] M.D. McKee, A. Nanci, W.J. Landis, Y. Gotoh, L.C. Gerstenfeld, M.J. Glimcher, Developmental appearance and ultrastructural immunolocalization of a major 66 kDa phosphoprotein in embryonic and post-natal chicken bone, Anat. Rec. 228 (1990) 77–92.
[19] M.D. McKee, A. Nanci, W.J. Landis, L.C. Gerstenfeld, Y. Gotoh, M.J. Glimcher, Ultrastructural immunolocalization of a major phosphoprotein in embryonic chick bone, Connect. Tissue Res. 21 (1989) 351–359.
[20] A.L. Arsenault, Structural and chemical analyses of mineralization using the turkey leg tendon as a model tissue, Bone Miner. 17 (1992) 253–256.
[21] H.A. Goldberg, G.K. Hunter, The inhibitory activity of osteopontin on hydroxyapatite formation in vitro, Ann. N. Y. Acad. Sci. 760 (1995) 305–308.
[22] D.T. Gilmour, G.J. Lyon, M.B. Carlton, J.R. Sanes, J.M. Cunningham, J.R. Anderson, B.L. Hogan, M.J. Evans, W.H. Colledge, Mice deficient for the secreted glycoprotein SPARC/osteonectin/BM40 develop normally but show severe age-onset cataract formation and disruption of the lens, EMBO J. 17 (1998) 1860–1870.
[23] S.R. Rittling, H.N. Matsumoto, M.D. McKee, A. Nanci, X.R. An, K.E. Novick, A.J. Kowalski, M. Noda, D.T. Denhardt, Mice lacking osteopontin show normal development and bone structure but display altered osteoclast formation in vitro, J. Bone Miner. Res. 13 (1998) 1101–1111.
[24] E. Holm, J.E. Aubin, G.K. Hunter, F. Beier, H.A. Goldberg, Loss of bone sialoprotein leads to impaired endochondral bone development and mineralization, Bone 71 (2015) 145–154.
[25] A.L. Boskey, S. Gadaleta, C. Gundberg, S.B. Doty, P. Ducy, G. Karsenty, Fourier transform infrared microspectroscopic analysis of bones of osteocalcin-deficient mice provides insight into the function of osteocalcin, Bone 23 (1998) 187–196.
[26] P. Ducy, C. Desbois, B. Boyce, G. Pinero, B. Story, C. Dunstan, E. Smith, J. Bonadio, S. Goldstein, C. Gundberg, A. Bradley, G. Karsenty, Increased bone formation in osteocalcin-deficient mice, Nature 382 (1996) 448–452.
[27] W.J. Landis, A study of calcification in the leg tendons from the domestic turkey, J. Ultrastruct. Mol. Struct. Res. 94 (1986) 217–238.
[28] J.X. Zhu, Y. Sasano, I. Takahashi, I. Mizoguchi, M. Kagayama, Temporal and spatial gene expression of major bone extracellular matrix molecules during embryonic mandibular osteogenesis in rats, Histochem. J. 33 (2001) 25–35.
[29] M.F. Young, J.M. Kerr, K. Ibaraki, A.M. Heegaard, P.G. Robey, Structure, expression, and regulation of the major noncollagenous matrix proteins of bone, Clin. Orthop. Relat. Res. 281 (1992) 275–294.
[30] E.A. Cowles, M.E. Derome, G. Pastizzo, L.L. Brailey, G.A. Gronowicz, Mineralization and the expression of matrix proteins during in vivo bone development, Calcif. Tissue Int. 62 (1998) 74–82.
[31] T. Nakase, K. Takaoka, K. Hirakawa, S. Hirota, T. Takemura, H. Onoue, K. Takebayashi, Y. Kitamura, S. Nomura, Alterations in the expression of osteonectin, osteopontin and osteocalcin mRNAs during the development of skeletal tissues in vivo, Bone Miner. 26 (1994) 109–122.
[32] Y. Sasano, Y. Maruya, H. Sato, J.X. Zhu, I. Takahashi, I. Mizoguchi, M. Kagayama, Distinctive expression of extracellular matrix molecules at mRNA and protein levels during formation of cellular and acellular cementum in the rat, Histochem. J. 33 (2001) 91–99.
[33] T. Takano-Yamamoto, T. Takemura, Y. Kitamura, S. Nomura, Site-specific expression of mRNAs for osteonectin, osteocalcin, and osteopontin revealed by in situ hybridization in rat periodontal ligament during physiological tooth movement, J. Histochem. Cytochem. 42 (1994) 885–896.
[34] P. Bianco, L.W. Fisher, M.F. Young, J.D. Termine, P.G. Robey, Expression of bone sialoprotein (BSP) in developing human tissues, Calcif. Tissue Int. 49 (1991) 421–426.
[35] J. Chen, H.S. Shapiro, J. Sodek, Development expression of bone sialoprotein mRNA in rat mineralized connective tissues, J. Bone Miner. Res. 7 (1992) 987–997.
[36] L.C. Gerstenfeld, J.B. Lian, Y. Gotoh, D.D. Lee, W.J. Landis, M.D. McKee, A. Nanci, M.J. Glimcher, Use of cultured embryonic chicken osteoblasts as a model of cellular differentiation and bone mineralization, Connect. Tissue Res. 21 (1989) 545–555.
[37] L.M. Siperko, R. Jacquet, W.J. Landis, Modified aminosilane substrates to evaluate osteoblast attachment, growth, and gene expression in vitro, J. Biomed. Mater. Res. A 78 (2006) 808–822.
[38] M. Weitzhandler, D.A. Carrino, A.I. Caplan, Proteoglycans synthesized during the cartilage to bone transition in developing chick embryos, Bone 9 (1988) 225–233.
[39] T. Miyake, A.M. Cameron, B.K. Hall, Stage-specific expression patterns of alkaline phosphatase during development of the first arch skeleton in inbred C57BL/6 mouse embryos, J. Anat. 190 (1997) 239–260.
[40] C. Vogel, E.M. Marcotte, Insights into the regulation of protein abundance from proteomic and transcriptomic analyses, Nat. Rev. Genet. 13 (2012) 227–232.
[41] M. Gry, R. Rimini, S. Stromberg, A. Asplund, F. Ponten, M. Uhlen, P. Nilsson, Correlations between RNA and protein expression profiles in 23 human cell lines, BMC Genomics 10 (2009) 365.
[42] L.C. Johnson, Mineralization of turkey leg tendon. I. Histology and histochemistry of mineralization, in: R.F. Sognnaes (Ed.), Calcification in Biological Systems, Am. Assn. Adv. Sci. 1960, pp. 117–128 Washington, DC.
[43] M.J. Nylen, D.B. Scott, V.M. Mosely, Mineralization of turkey leg tendon. II. Collagen–mineral relations as revealed by electron and X-ray microscopy, in: R.F. Sognnaes (Ed.), Calcification in Biological Systems, Am. Assn. Adv. Sci. 1960, pp. 129–142 Washington DC.
[44] R.C. Likens, Mineralization of turkey leg tendon. III. Chemical nature of the protein and mineral phases, in: R.F. Sognnaes (Ed.), Calcification in Biological Systems, Am. Assn. Adv. Sci. 1960, pp. 143–149 Washington DC.
[45] A.L. Arsenault, Crystal-collagen relationships in calcified turkey leg tendons visualized by selected-area dark field electron microscopy, Calcif. Tissue Int. 43 (1988) 202–212.
[46] A. Bigi, A. Ripamonti, M.H.J. Koch, N. Roveri, Calcified turkey leg tendon as structural model for bone mineralization, Int. J. Biol. Macromol. 10 (1988) 282–286.
[47] A.L. Arsenault, B.W. Frankland, F.P. Ottensmeyer, Vectorial sequence of mineralization in the turkey leg tendon determined by electron microscopic imaging, Calcif. Tissue Int. 48 (1991) 46–55.
[48] A.L. Arsenault, Image analysis of collagen-associated mineral distribution in cryogenically prepared turkey leg tendons, Calcif. Tissue Int. 48 (1991) 56–62.
[49] W.J. Landis, M.J. Song, A. Leith, L. McEwen, B. McEwen, Mineral and organic matrix interaction in normally calcifying tendon visualized in three dimensions by high voltage electron microscopic tomography and graphic image reconstruction, J. Struct. Biol. 110 (1993) 39–54.
[50] W.J. Landis, F.H. Silver, The structure and function of normally mineralizing avian tendons, Comp. Biochem. Phys. A 133 (2002) 1135–1157.
[51] J. Christoffersen, W.J. Landis, A contribution with review to the description of mineralization of bone and other calcified tissues in vivo, Anat. Rec. 230 (1991) 435–450.
[52] L. Chen, R. Jacquet, E. Lowder, W.J. Landis, Refinement of collagen-mineral interaction: a possible role for osteocalcin in apatite crystal nucleation, growth and development, Bone 71 (2015) 7–16.
[53] W.J. Landis, B.L.H. Kraus, C.A. Kirker-Head, Vascular-mineral spatial correlation in the calcifying turkey leg tendon, Connect. Tissue Res. 43 (2002) 595–605.
[54] J.C. Tank, D.S. Weiner, R. Jacquet, D. Childs, T.F. Ritzman, W.I. Horne, R. Steiner, M.A. Morscher, W.J. Landis, The effects of hypothyroidism on the proximal femoral physis in miniature swine, J. Orthop. Res. 31 (2013) 1986–1991.
[55] T. Scharschmidt, R. Jacquet, D. Weiner, E. Lowder, T. Schrickel, W.J. Landis, Gene expression in slipped capital femoral epiphysis. Evaluation with laser capture

microdissection and quantitative reverse transcription-polymerase chain reaction, J. Bone Joint Surg. Am. 91 (2009) 366–377.
[56] I. Rieu, S.J. Powers, Real-time quantitative RT-PCR: design, calculations, and statistics, Plant Cell 21 (2009) 1031–1033.
[57] E.B. Harvey, H.E. Kaiser, L.E. Rosenberg, An Atlas of the Domestic Turkey (*Meleagris gallopavo*): Myology and Osteology, U.S. Atomic Energy Commission, Division of Biology and Medicine, Washington DC, 1968, p. 105.
[58] E. Kärner, C.-M. Bäckesjö, J. Cedervall, R.V. Sugars, L. Ahrlund-Richter, M. Wendel, Dynamics of gene expression during bone matrix formation in osteogenic cultures derived from human embryonic stem cells in vitro, Biochim. Biophys. Acta 1790 (2009) 110–118.
[59] L.F. Cooper, P.K. Yliheikkilä, D.A. Felton, S.W. Whitson, Spatiotemporal assessment of fetal bovine osteoblast culture differentiation indicates a role for BSP in promoting differentiation, J. Bone Miner. Res. 13 (1998) 620–632.
[60] J.A.R. Gordon, C.E. Tye, A.V. Sampaio, T.M. Underhill, G.K. Hunter, H.A. Goldberg, Bone sialoprotein expression enhances osteoblast differentiation and matrix mineralization in vitro, Bone 41 (2007) 462–473.
[61] M. van Driel, M. Koedam, C.J. Buurman, M. Roelse, F. Weyts, H. Chiba, A.G. Uitterlinden, H.A.P. Pols, J.P.T.M. van Leeuwen, Evidence that both 1α,25-dihydroxyvitamin D3 and 24-hydroxylated D3 enhance human osteoblast differentiation and mineralization, J. Cell. Biochem. 99 (2006) 922–935.
[62] W. Huang, B. Carlsen, G. Rudkin, M. Berry, K. Ishida, D.T. Yamaguchi, T.A. Miller, Osteopontin is a negative regulator of proliferation and differentiation in MC3T3-E1 pre-osteoblastic cells, Bone 34 (2004) 799–808.
[63] J.Y. Choi, B.H. Lee, K.B. Song, R.W. Park, I.S. Kim, K.Y. Sohn, J.S. Jo, H.M. Ryoo, Expression patterns of bone-related proteins during osteoblastic differentiation in MC3T3-E1 cells, J. Cell. Biochem. 61 (1996) 609–618.
[64] L.C. Gerstenfeld, Y. Gotoh, M.D. McKee, A. Nanci, W.J. Landis, M.J. Glimcher, Expression and ultrastructural immunolocalization of a major 66 kDa phosphoprotein synthesized by chicken osteoblasts during mineralization in vitro, Anat. Rec. 228 (1990) 93–103.
[65] B. Ganss, R.H. Kim, J. Sodek, Bone sialoprotein, Crit. Rev. Oral Biol. Med. 10 (1999) 79–98.
[66] N. Harris, K. Rattray, C. Tye, T. Underhill, M. Somerman, J. D'Errico, A. Chambers, G. Hunter, H. Goldberg, Functional analysis of bone sialoprotein: identification of the hydroxyapatite-nucleating and cell-binding domains by recombinant peptide expression and site-directed mutagenesis, Bone 27 (2000) 795–802.
[67] C. Tye, K. Rattray, K. Warner, J. Gordon, J. Sodek, G. Hunter, H. Goldberg, Delineation of the hydroxyapatite-nucleating domains of bone sialoprotein, J. Biol. Chem. 278 (2003) 7949–7955.
[68] G.S. Baht, G.K. Hunter, H.A. Goldberg, Bone sialoprotein-collagen interaction promotes hydroxyapatite nucleation, Matrix Biol. 27 (2008) 600–608.
[69] S. Kasugai, R. Todescan Jr., T. Nagata, K.L. Yao, W.T. Butler, J. Sodek, Expression of bone matrix proteins associated with mineralized tissue formation by adult rat bone marrow cells in vitro: inductive effects of dexamethasone on the osteoblastic phenotype, J. Cell. Physiol. 147 (1991) 111–120.
[70] A.J. Camarda, W.T. Butler, R.D. Finkelman, A. Nanci, Immunocytochemical localization of gamma-carboxyglutamic acid-containing proteins (osteocalcin) in rat bone and dentin, Calcif. Tissue Int. 40 (1987) 349–355.
[71] M.D. McKee, M.J. Glimcher, A. Nanci, High-resolution immunolocalization of osteopontin and osteocalcin in bone and cartilage during endochondral ossification in the chicken tibia, Anat. Rec. 234 (1992) 479–492.
[72] J. Sodek, B. Ganss, M.D. McKee, Osteopontin, Crit. Rev. Oral Biol. Med. 11 (2000) 279–303.
[73] W.T. Butler, The nature and significance of osteopontin, Connect. Tissue Res. 23 (1989) 123–136.
[74] S. Nomura, A.J. Wills, D.R. Edwards, J.K. Heath, B.L. Hogan, Developmental expression of 2ar (osteopontin) and SPARC (osteonectin) RNA as revealed by in situ hybridization, J. Cell Biol. 106 (1988) 441–450.
[75] G.K. Hunter, C.L. Kyle, H.A. Goldberg, Modulation of crystal formation by bone phosphoproteins: structural specificity of the osteopontin-mediated inhibition of hydroxyapatite formation, Biochem. J. 300 (1994) 723–728.
[76] D.E. Rodriguez, T. Thula-Mata, E.J. Toro, Y.-W. Yeh, C. Holt, L.S. Holliday, L.B. Gower, Multifunctional role of osteopontin in directing intrafibrillar mineralization of collagen and activation of osteoclasts, Acta Biomater. 10 (2014) 494–507.
[77] P.V. Hauschka, J.B. Lian, D.E. Cole, C.M. Gundberg, Osteocalcin and matrix Gla protein: vitamin K-dependent proteins in bone, Physiol. Rev. 69 (1989) 990–1047.
[78] P.A. Price, S.K. Nishimoto, Radioimmunoassay for the vitamin K-dependent protein of bone and its discovery in plasma, Proc. Natl. Acad. Sci. U.S.A. 77 (1980) 2234–2238.
[79] P.A. Price, J.G. Parthemore, L.J. Deftos, New biochemical marker for bone metabolism. Measurement by radioimmunoassay of bone GLA protein in the plasma of normal subjects and patients with bone disease, J. Clin. Invest. 66 (1980) 878–883.
[80] P.A. Price, S.A. Baukol, 1,25-Dihydroxyvitamin D3 increases synthesis of the vitamin K-dependent bone protein by osteosarcoma cells, J. Biol. Chem. 255 (1980) 11660–11663.
[81] A.L. Bronckers, S. Gay, R.D. Finkelman, W.T. Butler, Developmental appearance of Gla proteins (osteocalcin) and alkaline phosphatase in tooth germs and bones of the rat, Bone Miner. 2 (1987) 361–373.
[82] B. Auf'mkolk, P.V. Hauschka, E.R. Schwartz, Characterization of human bone cells in culture, Calcif. Tissue Int. 37 (1985) 228–235.
[83] M.A. Aronow, L.C. Gerstenfeld, T.A. Owen, M.S. Tassinari, G.S. Stein, J.B. Lian, Factors that promote progressive development of the osteoblast phenotype in cultured fetal rat calvaria cells, J. Cell. Physiol. 143 (1990) 213–221.
[84] M.D. McKee, A. Nanci, S.R. Khan, Ultrastructural immunodetection of osteopontin and osteocalcin as major matrix components of renal calculi, J. Bone Miner. Res. 10 (1995) 1913–1929.
[85] K. Flade, C. Lau, M. Mertig, W. Pompe, Osteocalcin-controlled dissolution-reprecipitation of calcium phosphate under biomimetic conditions, Chem. Mater. 13 (2001) 3596–3602.
[86] R. Fujisawa, Y. Kuboki, Affinity of bone sialoprotein and several other bone and dentin acidic proteins to collagen fibrils, Calcif. Tissue Int. 51 (1992) 438–442.
[87] N. Arai, K. Ohya, S. Kasugai, H. Shimokawa, S. Ohida, H. Ogura, T. Amagasa, Expression of bone sialoprotein mRNA during bone formation and resorption induced by colchicine in rat tibial bone marrow cavity, J. Bone Miner. Res. 10 (1995) 1209–1217.
[88] L. Xu, Z. Zhang, X. Sun, J. Wang, W. Xu, L. Shi, J. Lu, J. Tang, J. Liu, X. Su, Glycosylation status of bone sialoprotein and its role in mineralization, Exp. Cell Res. 360 (2017) 413–420.
[89] Y. Yang, Q. Cui, N. Sahai, How does bone sialoprotein promote the nucleation of hydroxyapatite? A molecular dynamics study using model peptides of different conformations, Langmuir 26 (2010) 9848–9859.
[90] Y. Yang, D. Mkhonto, Q. Cui, N. Sahai, Theoretical study of bone sialoprotein in bone biomineralization, Cells Tissues Organs 194 (2011) 182–187.
[91] P.V. Hauschka, Osteocalcin: the vitamin K-dependent Ca^{2+}-binding protein of bone matrix, Haemostasis 16 (1986) 258–272.
[92] A.L. Bronckers, S. Gay, R.D. Finkelman, W.T. Butler, Immunolocalization of Gla proteins (osteocalcin) in rat tooth germs: comparison between indirect immunofluorescence, peroxidase-antiperoxidase, avidin-biotin-peroxidase complex, and avidin-biotin-gold complex with silver enhancement, J. Histochem. Cytochem. 35 (1987) 825–830.
[93] M.P. Mark, W.T. Butler, C.W. Prince, R.D. Finkelman, J.V. Ruch, Developmental expression of 44-kDa bone phosphoprotein (osteopontin) and bone gamma-carboxyglutamic acid (Gla)-containing protein (osteocalcin) in calcifying tissues of rat, Differentiation 37 (1988) 123–136.
[94] T. Sugiyama, S. Kawai, Carboxylation of osteocalcin may be related to bone quality: a possible mechanism of bone fracture prevention by vitamin K, J. Bone Miner. Metab. 19 (2001) 146–149.
[95] Q.Q. Hoang, F. Sicheri, A.J. Howard, D.S.C. Yang, Bone recognition mechanism of porcine osteocalcin from crystal structure, Nature 425 (2003) 977–980.
[96] A.J. Lee, S. Hodges, R. Eastell, Measurement of osteocalcin, Ann. Clin. Biochem. 37 (2000) 432–446.
[97] N.K. Lee, H. Sowa, E. Hinoi, M. Ferron, J.D. Ahn, C. Confavreux, R. Dacquin, P.J. Mee, M.D. McKee, D.Y. Jung, Z. Zhang, J.K. Kim, F. Mauvais-Jarvis, P. Ducy, G. Karsenty, Endocrine regulation of energy metabolism by the skeleton, Cell 130 (2007) 456–469.
[98] M. Ferron, E. Hinoi, G. Karsenty, P. Ducy, Osteocalcin differentially regulates beta cell and adipocyte gene expression and affects the development of metabolic diseases in wild-type mice, Proc. Natl. Acad. Sci. U. S. A. 105 (2008) 5266–5270.
[99] F. Oury, L. Khrimian, C.A. Denny, A. Gardin, A. Chamouni, N. Goeden, Y.Y. Huang, H. Lee, P. Srinivas, X.B. Gao, S. Suyama, T. Langer, J.J. Mann, T.L. Horvath, A. Bonnin, G. Karsenty, Maternal and offspring pools of osteocalcin influence brain development and functions, Cell 155 (2013) 228–241.
[100] I. Levinger, D. Scott, G.C. Nicholson, A.L. Stuart, G. Duque, T. McCorquodale, M. Herrmann, P.R. Ebeling, K.M. Sanders, Undercarboxylated osteocalcin, muscle strength and indices of bone health in older women, Bone 64 (2014) 8–12.
[101] Z.J. Chen, S.M. Huang, W.X. Fan, W.X. Tang, F. Liu, H.Y. Qiu, Effects of high glucose on expression of core binding factor alpha1 and osteocalcin in vascular smooth muscle cells, Sichuan Da Xue Xue Bao Yi Xue Ban 41 (2010) 784–788.
[102] L. Malaval, D. Modrowski, A.K. Gupta, J.E. Aubin, Cellular expression of bone-related proteins during in vitro osteogenesis in rat bone marrow stromal cell cultures, J. Cell. Physiol. 158 (1994) 555–572.
[103] L. Malaval, F. Liu, P. Roche, J.E. Aubin, Kinetics of osteoprogenitor proliferation and osteoblast differentiation in vitro, J. Cell. Biochem. 74 (1999) 616–627.
[104] M.J. Glimcher, Bone: nature of the calcium phosphate crystals and cellular, structural, and physical chemical mechanisms in their formation, Rev. Miner. Geochem. 64 (2006) 223–282.
[105] C. Burger, H. Zhou, H. Wang, I. Sics, B.S. Hsiao, B. Chu, L. Graham, M.J. Glimcher, Lateral packing of mineral crystals in bone collagen fibrils, Biophys. J. 95 (2008) 1985–1992.
[106] N. Lian, W. Wang, L. Li, F. Elefteriou, X. Yang, Vimentin inhibits ATF4-mediated osteocalcin transcription and osteoblast differentiation, J. Biol. Chem. 284 (2009) 30518–30525.
[107] N. Lian, T. Lin, W. Liu, W. Wang, L. Li, S. Sun, J.S. Nyman, X. Yang, Transforming growth factor beta suppresses osteoblast differentiation via the vimentin activating transcription factor 4 (ATF4) axis, J. Biol. Chem. 287 (2012) 35975–35984.
[108] M. Guo, A.J. Ehrlicher, S. Mahammad, H. Fabich, M.H. Jensen, J.R. Moore, J.J. Fredberg, R.D. Goldman, The role of vimentin intermediate filaments in cortical and cytoplasmic mechanics. Biophys. J. 105 (2013) 1562–1568.
[109] G.T. Charras, M.A. Horton, Single cell mechanotransduction and its modulation analyzed by atomic force microscope indentation, Biophys. J. 82 (2002) 2970–2981.
[110] W.M. Jackson, M.J. Jaasma, R.Y. Tang, T.M. Keaveny, Mechanical loading by fluid shear is sufficient to alter the cytoskeletal composition of osteoblastic cells, Am. J. Physiol. Cell Physiol. 295 (2008) C1007–C1015.
[111] W.J. Landis, K.J. Hodgens, D. Block, C.D. Toma, L.C. Gerstenfeld, Spaceflight effects on cultured embryonic chick bone cells, J. Bone Miner. Res. 15 (2000) 1099–1112.
[112] M.C. Meazzini, C.D. Toma, J.L. Schaffer, M.L. Gray, L.C. Gerstenfeld, Osteoblast cytoskeletal modulation in response to mechanical strain in vitro, J. Orthop. Res.

16 (1998) 170–180.
[113] Y. Kumei, S. Morita, H. Katano, H. Akiyama, M. Hirano, K. Oyha, H. Shimokawa, Microgravity signal ensnarls cell adhesion, cytoskeleton, and matrix proteins of rat osteoblasts: osteopontin, CD44, osteonectin, and alpha-tubulin, Ann. N. Y. Acad. Sci. 1090 (2006) 311–317.
[114] S. Zhou, Y. Zu, Z. Sun, F. Zhuang, C. Yang, Effects of hypergravity on osteopontin expression in osteoblasts, PLoS ONE 10 (2015) e0128846(8846).
[115] W. Zhang, P. Wei, Y. Chen, L. Yang, C. Jiang, P. Jiang, D. Chen, Down-regulated expression of vimentin induced by mechanical stress in fibroblasts derived from patients with ossification of the posterior longitudinal ligament, Eur. Spine J. 23 (2014) 2410–2415.
[116] J.P. Orgel, A. Eid, O. Antipova, J. Bella, J.E. Scott, Decorin core protein (decoron) shape complements collagen fibril surface structure and mediates its binding, PLoS One 4 (2009) e7028.
[117] K. Hoshi, S. Kemmotsu, Y. Takeuchi, N. Amizuka, H. Ozawa, The primary calcification in bones follows removal of decorin and fusion of collagen fibrils, J. Bone Miner. Res. 14 (1999) 273–280.
[118] I. Axelsson, J.C. Pita, D.S. Howell, R. Lorentzon, I. Berman, L. Boquist, Kinetics of proteoglycans and cells in growth plate of normal, diabetic, and malnourished rats, Pediatr. Res. 27 (1990) 41–44.